Anthony, Elizabeth Youngblood

GEOCHEMICAL EVIDENCE FOR CRUSTAL MELTING IN THE ORIGIN OF THE IGNEOUS SUITE AT THE SIERRITA PORPHYRY COPPER DEPOSIT, SOUTHEASTERN ARIZONA

The University of Arizona PH.D. 1986

PLEASE NOTE:

In all cases this material has been filmed in the best possible way from the available copy. Problems encountered with this document have been identified here with a check mark __✓__.

1. Glossy photographs or pages _____
2. Colored illustrations, paper or print _____
3. Photographs with dark background _____
4. Illustrations are poor copy _____
5. Pages with black marks, not original copy _____
6. Print shows through as there is text on both sides of page _____
7. Indistinct, broken or small print on several pages ✓
8. Print exceeds margin requirements _____
9. Tightly bound copy with print lost in spine _____
10. Computer printout pages with indistinct print _____
11. Page(s) _____ lacking when material received, and not available from school or author.
12. Page(s) _____ seem to be missing in numbering only as text follows.
13. Two pages numbered _____. Text follows.
14. Curling and wrinkled pages _____
15. Dissertation contains pages with print at a slant, filmed as received _____
16. Other _____

_____

_____

GEOCHEMICAL EVIDENCE FOR CRUSTAL MELTING IN THE ORIGIN OF THE IGNEOUS SUITE AT THE SIERRITA PORPHYRY COPPER DEPOSIT, SOUTHEASTERN ARIZONA

by

Elizabeth Youngblood Anthony

A Dissertation Submitted to the Faculty of the

DEPARTMENT OF GEOSCIENCES

In Partial Fulfillment of the Requirements
For the Degree of

DOCTOR OF PHILOSOPHY

In the Graduate College

THE UNIVERSITY OF ARIZONA

1 9 8 6

THE UNIVERSITY OF ARIZONA
GRADUATE COLLEGE

As members of the Final Examination Committee, we certify that we have read the dissertation prepared by Elizabeth Youngblood Anthony

entitled Geochemical evidence for crustal melting in the origin of the igneous suite at the Sierrita porphyry copper deposit, Arizona

and recommend that it be accepted as fulfilling the dissertation requirement for the Degree of Doctor of Philosophy.

Spencer R. Titley	April 16, 1986 Date
D. Granguly	April 18, 1986 Date
Porth	24 Apr 86 Date
Richard J. Drake	24 April 86 Date
	24 April 86 Date

Final approval and acceptance of this dissertation is contingent upon the candidate's submission of the final copy of the dissertation to the Graduate College.

I hereby certify that I have read this dissertation prepared under my direction and recommend that it be accepted as fulfilling the dissertation requirement.

Spencer R. Titley	April 16, 1986
Dissertation Director	Date

STATEMENT BY AUTHOR

This dissertation has been submitted in partial fulfillment of requirements for an advanced degree at The University of Arizona and is deposited in the University Library to be made available to borrowers under rules of the Library.

Brief quotations from this dissertation are allowable without special permission, provided that accurate acknowledgment of source is made. Requests for permission for extended quotation from or reproduction of this manuscript in whole or in part may be granted by the head of the major department or the Dean of the Graduate College when in his or her judgment the proposed use of the material is in the interests of scholarship. In all other instances, however, permission must be obtained from the author.

SIGNED: Elizabeth Greyblood Arthur

ACKNOWLEDGEMENTS

This study was made possible by the use of the excellent facilities provided in the Gamma-Ray Laboratory, under the direction of William Boynton, and the isotope laboratory of Jon Patchett and Paul Damon. Drs. Boynton and Patchett spent many hours teaching me how to use their labs and how to interpret the results, and I have enjoyed and appreciated the time.

Also, I am indebted to Nancy Hess, who analyzed and interpreted the compositions of the mafic minerals, and Rick Trapp, who meticulously prepared samples for crushing and assisted during neutron activation analysis. Nancy's use of the SEMQ laboratory, under the ever-patient ministrations of Tom Teska, is gratefully acknowledged. Darby Dyar, Kurt Fredriksson, and Eugene Jarosewich analyzed some of the biotites for their ferrous/ferric ratios, information which is crucial to determination of the oxygen fugacities.

Paula Davidson and Terry Wallace taught me inverse methods. Each has the art of making the seemingly complex understandable.

The study has benefitted from conversations with Lee Silver, Philip Candela, Wayne Burnham, Donald DePaolo, Charles Meyer, Nancy Hess, Chris Eastoe, and through it

all, John Anthony. I acknowledge particularly the contributions of Wayne Burnham, because his ideas of the igneous regime associated with metallogenesis have been very influential, and of Donald DePaolo for his explanations of coupled assimilation and differentiation. The manuscript has been made materially better by helpful reviews from my committee members, Jiba Ganguly, Mike Drake, Joaquin Ruiz, and Jon Patchett.

And finally, my greatest debt is to my advisor, Spencer Titley. His wise recognition of the problem and his choice of the specific area, Sierrita, has been what made the study successful. He has been a great pleasure to work with because he allows me to explore avenues in my own way, while always remaining available for counsel. And his counsel is invariably well-considered and scientifically provocative.

The study was funded by National Science Foundation Grant EAR 8218875 to Dr. Titley.

TABLE OF CONTENTS

TABLE OF CONTENTS--continued

LIST OF ILLUSTRATIONS

LIST OF TABLES

ABSTRACT

Numerical values for parameters which characterize melting regimes and differentiation history have been determined for a suite of genetically-related calc-alkaline rocks. Isotopic ratios of Nd and Sr vary sympathetically, with the least differentiated and oldest rocks having $\varepsilon_{Nd} = -4.3$ and $^{87}/Sr^{86}Sr_o = 0.7069$ and the most differentiated and youngest characterized by $\varepsilon_{Nd} = -8.5$ and $^{87}Sr/^{87}/Sr_o = 0.7092$. These observations imply that a process which might relate the various units is that of invasion of the crust by mantle-derived magmas and progressive assimilation.

The most negative Nd values may well represent the isotopic signature of the crustal rocks which melted. Melting of a 1.8 Ga source region (an age characteristic of the basement in southeastern Arizona) which had a $^{147}Sm/^{144}Nd$ ratio of .13 would yield Laramide melts with an ε_{Nd} of -8.5. This Sm/Nd ratio is characteristic of a somewhat mafic (lower?) crust, a character consistent with petrological and chemical evidence which suggest that the source was intermediate to mafic in composition and of amphibolite grade.

Solution of the isotopic data yields a value of r (the instantaneous ratio of assimilated material to

crystallizing magma) equal to Ø.6 to Ø.9. These values are reasonable considering heat budgets of crystallization and fusion in the lower crust. Solution of the set of equations for changes in concentration of the trace elements yields numeric values for the f, fraction of remaining melt for each unit in the series. The values are: andesite, f-Ø.63; granodiorite, f-Ø.42 to Ø.32; and the final granite stocks and dikes, f-Ø.34.

The modelling provides insight into the way an igneous suite intimately associated with copper mineralization has evolved. The porphyry ore bodies are related to long-lived and large magma systems. At the level of mineralization and observation, we sample only a small portion of the system. The importance of subduction to metallogenesis may be that it provides a heat source, in the form of mantle-derived magmas, which allows extensive melting of hydrous crust. Thus, as is becoming evident from other studies as well, assimilation and crustal anatexis are major processes in generating granitoid rocks at convergent plate boundaries.

CHAPTER 1

INTRODUCTION

Porphyry copper deposits are intrusion-related systems. Spatial and temporal association of mineralization with intrusions is indicated by the distribution of alteration and mineralization, which is centered upon small porphyritic bodies, and the similar ages of mineralization and igneous activity. Because of the relationships between ore and igneous rocks, understanding of metallogenesis requires knowledge of the igneous system. Although there have been studies of Pacific porphyry systems (Mason and McDonald, 1978, Hine and Mason, 1978, Whalen et al., 1982), there have been no detailed geochemical studies of magma provenance and igneous evolution in individual systems of the American Southwest. This kind of characterization is the subject of the present study.

The petrologic nature of these intrusions has been investigated in numerous studies, and summarized most recently in Titley and Beane (1981). They are porphyritic, with potassium feldspar the most common phenocryst, contain biotite and often hornblende, and the mafic minerals have quite elevated magnesium contents (Mason, 1978, Chivas,

1981, Whalen et al., 1982, Hess et al., in prep.) These characteristics imply that the magmas were oxidizing and hydrous, and would have contained the requisite properties to fracture host rocks, as well as the volume of copper and sulfur-rich fluid needed to initiate mineralization (Burnham, 1979, Burnham and Ohmoto, 1980). The chemical nature of the rocks varies with the tectonic setting of the deposit: the igneous suites in the Pacific arc deposits are more mafic (quartz diorite) than are those of the western United States, which are granodioritic to granitic in composition (Titley and Beane, 1981).

The intrusions are commonly shallow -- most estimates place them within 5 kilometers of the surface -- and they often intrude andesitic volcanic rocks. The volcanic rocks are commonly believed to be co-genetic with the intrusions, although there have been no reported isotopic or trace-element studies which test this assertion. The local volcanic environment reflects the regional tectonic setting of subduction (Titley and Beane, 1981). Most deposits are in the Pacific "ring of fire" or the Alpine belt, and the ages of mineralization are synchronous with active subduction -- Paleocene (Laramide) but not younger in the American Southwest, Paleocene through Pliocene for the South American deposits where subduction has been continuous, and not older than

Oligocene for the deposits of the Pacific islands, where convergence is thought to be quite recent.

One of the chief concerns is to elucidate how the igneous rocks acquired their characteristics. For instance, what is the significance of subduction to the generation of the melts, and how many of the crucial magmatic characteristics, such as an oxidizing and hydrous nature, are intrinsic to the source materials for the magmas, and how many are due to the crystallization history, such as depth of emplacement and timing of vapor exsolution? These questions also have bearing on the development of a general theory for metallogenesis of all intrusion-centered ore systems, including, tin, tungsten, molybdenum, and copper.

The present study was designed to address these questions by investigating the fundamental nature of the intrusive and volcanic rocks at the Sierrita-Esperanza deposit in the Pima district of southern Arizona. The aim of the study is to characterize both the crystallization history and the provenance of the magmas. This particular deposit was chosen because its hydrothermal history has been well-characterized (Titley et al., in press, Titley, 1982b), it contains a diverse suite of Laramide igneous rocks, and it has escaped the chemically pervasive quartz-sericite alteration, which makes possible the collection of unaltered samples.

The central questions addressed in the investigation are: 1) What kinds of rocks melted to produce the Laramide intrusive and volcanic suite; that is, what are the source materials for the magmas? Are they crustal or mantle? Strontium and neodymium isotopic and trace element compositions of the rocks are used to evaluate these questions. 2) Are the different units related to each other, and, if so, by what process are they related -- melting, differentiation, or assimilation? Inverse methods are used to obtain numeric solutions for certain parameters, such as fraction of melt and percent assimilation, which characterize the process. 3) How does the knowledge of magma genesis contribute to our understanding of ore genesis? Although this study does not directly address the bridge between magmatic and hydrothermal regimes, it provides constraints on the hypotheses set forth concerning that problem. Because of the tectonic setting of these deposits, the results of the study pertain as well to the general question of magmatism at convergent plate boundaries. Approximately thirty samples were collected from the major Laramide units in the area of the Sierrita-Esperanza deposit. The samples were analyzed for major-element chemistry by x-ray fluorescence and for trace-element compositions by instrumental neutron activation analysis; nine samples selected as representative of the chemical diversity in the suite were analyzed for their strontium

and neodymium isotopic compositions. In addition, a study was initiated to investigate compositions of the ferromagnesian minerals in the intrusive rocks of the suite in order to assess intensive parameters during crystallization.

CHAPTER 2

GEOLOGIC SETTING

The Sierrita-Esperanza porphyry copper deposit is part of a complex of orebodies in the Sierrita Mountains of southern Arizona, all of which are related to a Laramide intrusive episode. The geology of the district has been reviewed by various authors (Cooper, 1960, 1971, Titley, 1982b, West and Aiken, 1982). The reader is referred to these studies for more detailed descriptions of the field relations and petrography of the units.

Mineralization in the district consists of five productive skarn bodies and numerous small vein and replacement bodies and the disseminated copper and molybdenum of the Sierrita and Esperanza deposits. Combined reserves for the entire area are approximately 1.4×10^9 tons of Cu, Mo, and Ag ore (Titley, 1982b). This may be favorably compared with other great porphyry copper deposits and districts of the world, including the giant Chuquicamata deposit of Chile, with reserves of an estimated 8.8×10^9 tons, Cerro Colorado, Panama, with 2×10^9 tons, and Bingham, Utah, with 1.8×10^9 tons (Gilmour, 1982). The rocks about which this study is concerned -- those of the Sierrita

district -- have generated one of the pre-eminent intrusion-centered hydrothermal ore districts of the world.

The Sierrita Mountains comprise predominantly Mesozoic-aged igneous rocks of two different cycles (Figure 1). The first cycle consists of andesitic and rhyolitic volcanic rocks and granites having ages of 200 m.y. to 150 m.y. (Titley, 1982b), followed by a hiatus of igneous history from some 70 m.y. until the initiation of the Laramide igneous cycle at 68 m.y. ago.

The Laramide igneous cycle is the one of concern in this study. It commenced with emplacement of small plugs of quartz diorite intc early Mesozoic volcanic and volcaniclastic rocks and synchronous extrusion of andesitic volcanic rocks approximately 67-68 m.y. ago. This early stage was followed by intrusion of a batholithic granodiorite, the Ruby Star Granodiorite and related late-stage small plugs and dikes. The suite becomes increasingly more felsic with time. Descriptions of these rocks follow.

Quartz Diorite

The oldest intrusive rocks in the Laramide cycle are small plugs of quartz diorite. These crop out along a northwest trend (Figure 1). They are equigranular and have plagioclase, pyroxene, and hornblende as early phases. Fine-granied biotite occurs interstitially. Potassium

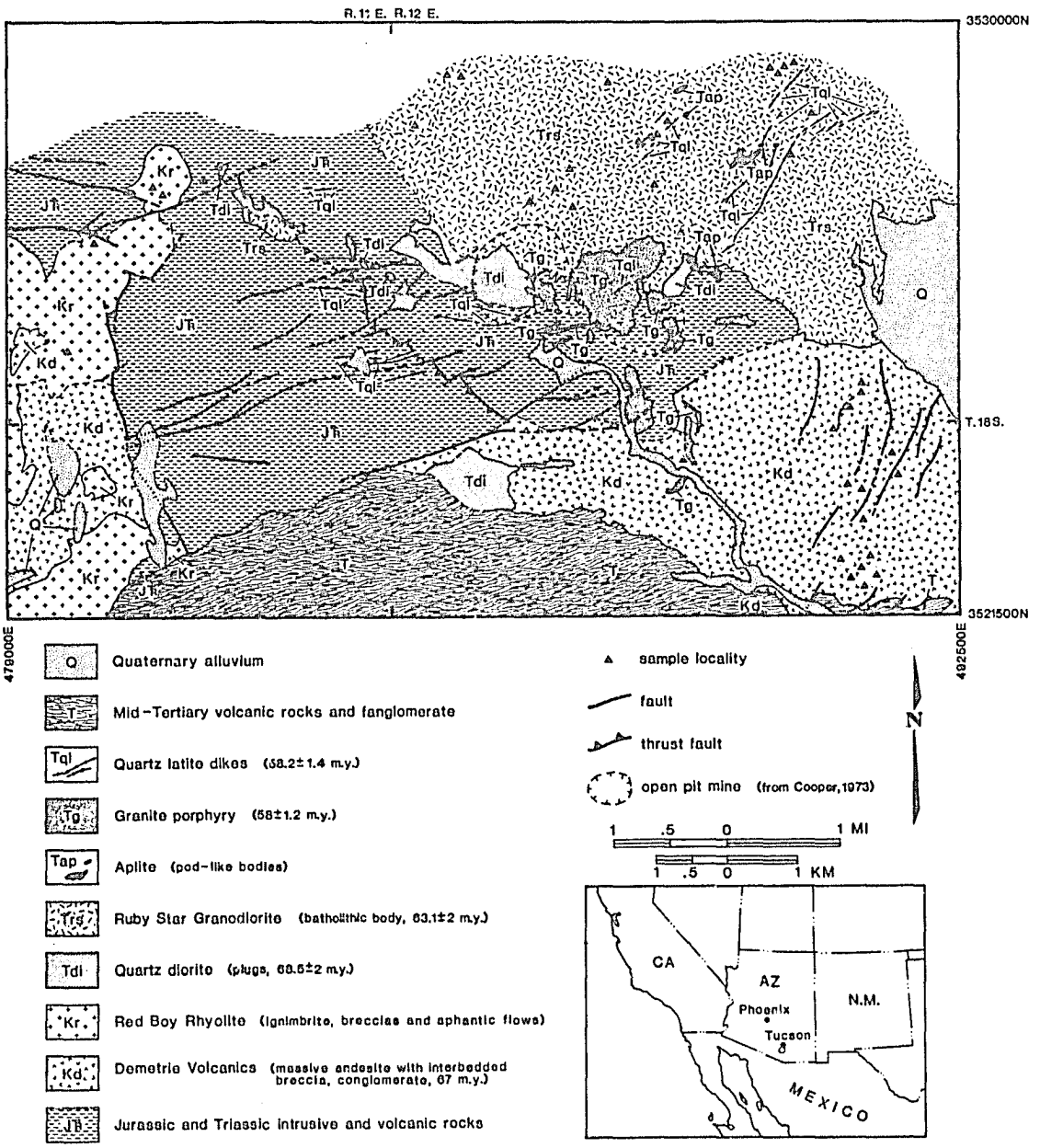

Figure 1. Geologic map of the Sierrita-Esperanza district from Cooper (1973) and Titley (1982b). Site of study located in circle south of Tucson on inset map.

feldspar is as growths on the plagioclase laths. Chemical and modal analyses for these may be found in Table 1.

Andesitic Volcanic Rocks

The Demetrie Volcanics were emplaced approximately 68 to 67 m.y. ago. The major portion of this unit is a massive and altered andesite having a purple matrix, plagioclase phenocrysts and remnants of hornblende and pyroxene phenocrysts (Table 1). The massive (i.e., not flow-lineated) character of outcrop and the phenocryst-rich nature of the rock (Table 1) suggest that it is a volcanic domal deposit (McBirney, 1983, personal communication). It is a high-K andesite according to its SiO_2 content (59-62 weight percent) and K_2O (2.9-3.5 weight percent). Rhyolites are present at both the top and bottom of the unit.

Stratigraphically above the andesite is the Red Boy Rhyolite, a unit which includes aphanitic flows, ignimbrites, and volcanic breccias. Its age has not been established; Cooper (1971) argues on the basis of regional correlation with other rhyolitic units that the Red Boy Rhyolite is approximately 70-65 m.y. old. That it is older than the granodiorite is demonstrated by the fact that fractures within the rhyolite are cross-cut by fractures generated by the granodiorite (Titley et al., in press). Its chemical nature, and relation to the main igneous cycle,

Table 1. Major element and modal analyses.

	DIORITE		ANDESITE					
	D-MR2-2	D-MR2-3	KD-GR2-7	KDR-GR2-9	KDGR-4	KD-GR2-5	6-81-2	KD-GR2-1
SiO2	59.30	60.90	62.70	61.90	59.20	57.90	60.70	61.10
TiO2	0.68	0.66	0.55	0.59	0.48	0.42	0.42	0.50
Al2O3	16.80	17.00	16.90	17.00	15.90	16.20	16.00	16.70
Fe2O3(T)	6.15	5.86	5.61	6.33	5.58	5.41	5.29	5.39
MnO	0.09	0.09	0.09	0.11	0.08	0.08	0.08	0.04
MgO	2.10	2.00	2.50	2.30	2.20	1.50	2.00	0.93
CaO	4.90	4.87	2.88	3.31	3.69	4.81	3.91	2.25
Na2O	3.87	3.85	4.77	4.23	3.71	4.02	3.38	4.55
K2O	3.39	3.58	3.65	3.80	3.66	3.60	3.00	4.27
P2O5	-	-	-	-	0.29	0.28	0.15	0.30
L.O.I.	-	-	-	-	5.08	4.93	4.15	3.23
Sum	97.27	98.81	99.64	99.63	99.87	99.15	99.08	99.25
D.I.	61.90	65.50	72.30	69.30	64.70	64.20	63.30	74.80
quartz	7.40		-**		-**	-**	-**	-**
K-spar	1.80		-		-	-	-	-
plag	76.80		36.00		43.00	41.00	43.00	43.00
opx	-		3.00			-	-	6.00
cpx	2.20		-		6.00	-	-	-
hbl	2.20		5.00		8.00	10.00	6.00	4.00
biot	6.80		-		-	3.00	3.00	-
titanite	-		tr		tr	-	tr	tr
zircon	tr		-		tr	tr	-	tr
epidote	0.20		-		-	-	-	-
apatite	tr		tr		tr	tr	tr	tr
magnetite	2.40		tr		tr	tr	tr	tr
rutile	tr		-		-	-	-	-
allanite	-	-	-	-	-	-	-	-
grndmass			61.00		43.00	46.00	48.00	47.00

a. Wet chemical analysis yields Fe2+/Fe(T)=0.50 (RS-MR-5); Fe2+/Fe(T)=0.48 (RS-MR3-8).
Modal analyses based on 500 points except those indicated by asterisks,
which are based on 200 points.

Table 1.(cont.)

	GRANODIORITE						LATE-STAGE BODIES		
	RS-MR-5	RSMR3-6	RSMR-8	RSMR3-2	RSMR3-5	RSMR3-8	QL-MR-7	TWB-PA	QL-85-1
SiO2	65.70	68.90	67.70	68.30	67.20	69.80	68.90	69.40	69.60
TiO2	0.42	0.41	0.41	0.36	0.41	0.28	0.37	0.31	0.36
Al2O3	15.60	15.70	15.70	16.00	16.00	15.40	15.30	15.60	15.20
Fe2O3(T)	3.37 a	3.17	3.13	2.92	2.87	2.27 a	2.89	1.89	1.76
MnO	0.05	0.03	0.04	0.02	0.04	0.04	0.03	0.03	0.02
MgO	1.20	0.90	0.89	0.81	0.88	0.65	0.80	0.73	0.78
CaO	3.16	2.66	2.79	2.34	2.67	2.05	2.20	2.22	1.34
Na2O	3.89	4.10	4.20	4.04	4.12	3.98	3.99	4.20	3.90
K2O	3.71	3.92	3.53	3.72	3.81	3.95	4.29	4.24	5.59
P2O5	-	-	-	-	-	-	-	0.11	0.14
L.O.I.	-	-	-	-	-	-	-	1.47	1.31
Sum	97.10	99.79	98.39	98.52	98.01	98.42	98.77	100.20	100.00
D.I.	74.50	80.12	78.50	79.40	78.40	82.60	82.00		
quartz	19.60	22.60	15.20		24.40	27.80	4.00*		
K-spar	24.20	21.40	9.80		21.00	20.40	-		
plag	48.00	49.00	65.60		43.20	45.00	22.00		
opx	-	-	-		-	-	-		
cpx	-	-	-		-	-	-		
hbl	0.20	-	1.00		0.80	-	-		
biot	5.40	6.00	6.20		7.80	5.20	6.00		
titanite	2.00	0.20	0.60		0.60	0.60	tr		
zircon	0.20	tr	0.20		tr	tr	tr		
epidote	-	-	-		tr	-	-		
apatite	tr	tr	0.20		0.40	0.20	tr		
magnetit	0.20	0.80	1.00		1.60	0.40	tr		
rutile	-	-	-		-	tr	-		
allanite	-	-	tr		tr	tr			
grndmass							68.00		

a. Wet chemical analysis yields Fe2+/Fe(T)=0.50 (RS-MR-5); Fe2+/Fe(T)=0.48 (RS-MR3-8).
Modal analyses based on 500 points except those indicated by asterisks,
which are based on 200 points.

Table 1.(cont.)

	APLITES AND RHYOLITES						ALTERED SAMPLES			
	RSMR-6	RSMR-4	KDR-GR-7	KR-MR2-4	KR-3	KR-2	RSMR3-3	RS-MR3-4	RS-SM-1	RS-SM-10
SiO2	76.70	69.60	74.70	73.00	75.60	76.30	63.30	60.80	65.80	70.50
TiO2	0.10	0.28	0.09	0.27	0.10	0.14	0.28	0.24	0.45	0.33
Al2O3	12.40	14.70	13.70	14.50	12.90	12.80	17.50	18.00	15.50	15.90
Fe2O3(T)	0.67	1.87	0.94	2.60	0.77	0.88	1.64	1.34	3.79	2.22
MnO		0.02	0.03	0.08	0.19	0.09	0.03	0.02	0.04	0.02
MgO	0.05	0.54	0.17	0.65	0.17	0.25	1.30	1.10	1.40	0.78
CaO	0.69	1.62	0.70	2.28	0.98	0.78	1.68	0.54	2.97	2.17
Na2O	2.92	3.64	3.38	2.95	5.93	5.15	3.63	2.26	3.86	4.04
K2O	5.51	5.28	5.48	4.16	2.44	3.09	8.11	12.62	2.80	4.40
P2O5	-	-	-	-	0.03	0.04	-	-	-	-
L.O.I.	-	-	-	-	1.23	0.77	-	-	-	-
Sum	99.04	97.55	99.20	100.49	100.34	100.29	97.48	96.92	96.61	100.35
D.I.	94.20	85.57	93.10	82.90			84.00	87.30	72.70	84.10
quartz	25.20	18.20						4.60	26.20	15.80
K-spar	34.40	15.00						46.80	17.80	22.00
plag	39.80	59.80						38.40	45.40	53.20
opx	-	-						-	-	-
cpx	-	-						-	-	-
hbl	-	-						tr	-	-
biot	tr	4.20						9.00	8.80	7.00
titanite	-	2.20						-	0.40	-
zircon	tr	tr						0.40	tr	tr
epidote	0.20	tr						-	-	1.00
apatite	tr	0.40						0.80	tr	0.20
magnetit	0.40	0.20						tr	1.40	0.40
rutile	tr	tr						tr	-	tr
allanite		tr	-				-	tr	-	0.20
grndmass										

a. Wet chemical analysis yields Fe2+/Fe(T)=0.50 (RS-MR-5); Fe2+/Fe(T)=0.48 (RS-MR3-8).
Modal analyses based on 500 points except those indicated by asterisks,
which are based on 200 points.

will be discussed in a later report (Anthony and Titley, in prep.).

Granodiorite

Emplacement of the Ruby Star Granodiorite occurred 63 m.y. ago. This body is elongate north-south and exhibits equigranular margins at both the east and west contacts. The equigranular samples are quartz monzodiorite and granodiorite according to their modal compositions (Streckeisen, 1973). The equigranular margin grades into a porphyritic center, which according to its modal classification is a granite. Mineralogy of both the equigranular and porphyritic phases (see Table 1, pp. 10-12) is characterized by early plagioclase feldspar, and zircon as inclusions within the plagioclase. Titanite and hornblende were next to crystallize, followed by potassium feldspar, quartz, and biotite. The porphyritic texture results from large (1-3 cm) potassium feldspar crystals. Exploratory drilling at Sierrita has shown that the granodiorite extends beneath the Jurassic rocks to the south.

Late-Stage Bodies

The granodiorite is cross-cut by dikes and small (ca. 1 km) plugs. The plugs (TWB-PA) are exposed within the open pits of the mine, and it is these bodies around which fracturing and mineralization is centro-symmetric.

They are characterized by a lack of mafic minerals, an aphanitic groundmass of quartz, potassium feldspar, and plagioclase, and potassium feldspar phenocrysts. The dikes are porphyritic with a fine-grained groundmass and plagioclase, orthoclase, and biotite phenocrysts.

Geochronology

Much of the discussion which follows concerning the genesis of these rocks is dependent upon a precise knowledge of the temporal relationships between the units. This section serves as a review of the geochronological data which are available for the district. It must be stressed at the outset of this review that the relative ages of the units are for the most part well-established by stratigraphy and field relations (Cooper, 1960, 1971, 1973). The granodiorite is clearly intrusive into the andesite, and the plugs and dikes are intrusive into the granodiorite body. The more problematic units, with respect to field relations, are the Red Boy Rhyolite and the quartz diorite. The rhyolite is in contact with Jurassic and Triassic rocks and the Demetrie Andesite. Cooper maps the contact between the andesite and the rhyolite as rhyolite deposited on andesite flows. This relationship, if correct, serves to give a maximum age of the rhyolite. The only constraint for a minimum age is the observation (Titley et al, in press) that fractures generated by the porphyry

bodies in the vicinity of the mines crosscut an earlier set of fractures which center on Red Boy Peak. Their conclusion is that Red Boy Peak was the location of an intrusive, hydrothermal event which preceded that related to the granite porphyry bodies and currently-exploited copper mineralization.

The quartz diorite is in contact with Jurassic intrusive rocks, the Ruby Star Granodiorite, and, in the open pit, the porphyry bodies. If it were to be intrusive with respect to all these units, it would be of Tertiary age, however, it is host to mineralization and two independent K-Ar ages place it as approximately synchronous with the Demetrie Andesite. Cooper (1960) also discusses the puzzling field relations of this rock.

Isotopic age dates for this district consist entirely of potassium-argon determinations, a technique which is not ideally suited to rocks of volcanic origin, or to those which have undergone the profound potassium metasomatism characteristic of the hydrothermal regime associated with mineralization. Despite these difficulties, most reported dates conform to what is known of the stratigraphy. The dates, their reported errors, and the material used to obtain the date, are summarized in Figure 2. The dates for the quartz diorite are from Cooper (1973) and Marvin et al. (1973), that for the Demetrie Andesite from Titley and Beane (1981), those from the Ruby Star Granodiorite

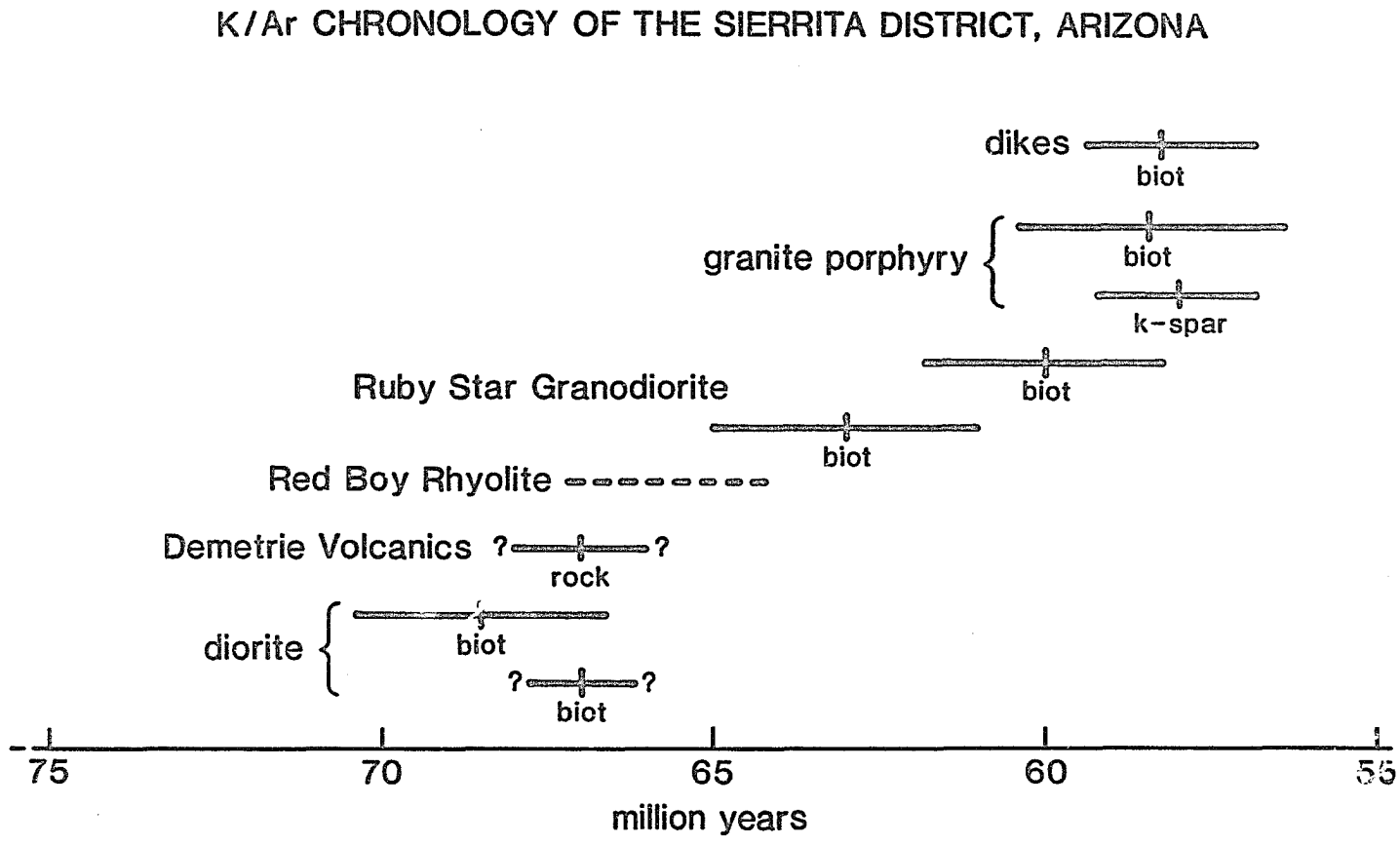

Figure 2. Geochronology of the units in the Sierrita-Esperanza district.

from Marvin et al. (1973) and Shafiquillah and Langlois (1978), that for the quartz latite dikes from the present study, and the two for the granite porphyry from Shafiquillah and Langlois (1978).

It is clear from Figure 2 (see p. 16) that volcanic rocks and the quartz diorite are the oldest rocks in the sequence, the granodiorite is intermediate, and the dikes and plugs are essentially synchronous. Thus the essential characteristics of the geochronology seem fairly well established. What is of less certainty, given the method of determination, is the exact duration of igneous activity. The ages imply a duration of ten million years, however, this is probably a maximum number, and the true duration could well be less.

CHAPTER 3

ANALYTICAL RESULTS

Samples of the rocks described, as well as mineral separates, were analyzed for their trace-element compositions using instrumental neutron activation analysis. Representative samples of specific units were analyzed for isotopic compositions using mass spectrometry. A description of the analytical techniques may be found in Appendix I, and the data are shown in Tables 2, 3, and 4.

Mineral separate analyses were carried out because of the uncertainty that exists as to whether whole rock compositions are representative of the liquids from which they crystallized. In order to assess the seriousness of that problem, minerals from one sample of equigranular granodiorite were analyzed; the results are shown in Table 2.

Mineral Separates

Amphibole, plagioclase, and titanite were separated by magnetic and density methods and analyzed; these minerals were chosen because they were the earliest to crystallize and thus control development of the trace-element patterns. Because the entire mineral was analyzed, the "K_d" reported in Table 2 is an average concentration relative to liquid

Table 2. Element concentrations for mineral separates. Values in ppm unless otherwise noted.

	RS-MR-5						
	WHOLE ROCK	TITANITE conc	"Kd"	HORNBLENDE conc	"Kd"	PLAGIOCLASE conc	"Kd"
Na %	2.89	1.34	0.46	0.52	0.18	3.22	1.11
K %	3.08		0.00		0.00		0.00
Ca %	2.38	18.41	7.74	8.59	3.61	2.36	0.99
Sc	5.03	12.54	2.49	120.80	24.02	0.10	0.02
Cr		51.31		25.65		0.54	
Mn	395.20						
Fe %	2.36	1.31	0.55	9.11	3.86	0.11	0.05
Co	8.49	2.32	0.27	55.54	6.54	0.43	0.05
Ni	11.87	122.70	10.34	61.49	5.18	1.29	0.11
Zn	42.09	99.77	2.37	291.40	6.92	6.45	0.15
Rb	146.45	n.d.		34.71	0.24	5.49	0.04
Sr	448.37	n.d.		15.74	0.04	512.50	1.14
Zr	132.25	1285	9.72	95.13	0.72	10.79	0.08
Mo		n.d.		n.d.		0.50	
Cs	3.97	n.d.		2.10	0.53	0.22	0.06
Ba	878.59	n.d.		50.99	0.06	140.70	0.16
La	34.21	n.d.		36.74	1.07	6.65	0.19
Ce	55.32	6976.9	126.12	57.55	1.04	5.57	0.10
Nd	21.31	3134.4	147.09	22.40	1.05	1.11	0.05
Sm	3.64	528.20	145.11	4.55	1.25	0.08	0.02
Eu	0.84	87.13	104.10	0.62	0.74	0.32	0.38
Gd	3.25	463.54	142.63	4.20	1.29		
Tb	0.33	51.46	155.47	0.53	1.61	0.01	0.02
Dy	1.29	257.40	199.53	4.59	3.56		
Ho	1.29	146.04	113.21	3.11	2.41	0.42	0.33
Tm		18.08		0.23			
Yb	0.98	127.80	130.41	2.06	2.10	0.02	0.03
Lu	0.17	17.70	102.91	0.40	2.31	0.003	0.02
Hf	4.07	68.93	16.94	3.99	0.98	0.15	0.04
Ta	0.74	133.20	181.22	0.26	0.36	0.01	0.02
Th	21.10	522.90	24.78	2.93	0.14	0.37	0.02
U	6.07	258.00	42.50	2.75	0.45	0.40	0.07

Table 3. Sm/Nd and Rb/Sr analyses.

	$^{143}Nd/^{144}Nd$	Sm	Nd	$^{143}Nd/^{144}Nd$	ϵ_{Nd}	$^{87}Sr/^{86}Sr_m$	Rb	Sr	$^{87}Sr/^{86}Sr$	ϵ_{Sr}	age
Diorite											
D-MR2-2	0.512223±6	5.85	32.52	0.512175	-7.3	0.708834±13	112.79	630.05	0.70834	55.64	67
Rhyolite											
KR-3	0.512261±5	4.26	15.87	0.512192	-7.1	0.712118±10	125.87	88.35	0.70831	55.18	65
Andesite											
KD-GR2-1	0.512381±5	4.95	27.82	0.512334	-4.3	0.707390±10	115.96	612.12	0.70686	34.74	67
KD-GR2-5	0.512381±5	4.67	25.48	0.512332	-4.3						
Granodiorite											
RS-MR-5	0.512265±4	3.39	20.64	0.512225	-6.5	0.708485±6	138.81	438.17	0.7077	46.14	62
RS-MR-5X	0.512247±7	3.30	20.21	0.512207	-6.9	0.708438±7	140.75	442.10	0.70763	45.42	62
RS-MR3-2	0.512204±7	3.46	21.62	0.512163	-7.7						62
FD(84)	0.512205	2.95	18.70	0.512167	-7.7	0.7097	177.2	360.	0.70347	57.33	61
Late-stage bodies											
TWB-PA	0.512173±5	3.83	23.78	0.512135	-8.3						60
QL-85-1	0.512164±6	3.96	24.09	0.512126	-8.5	0.710751±9	265.02	397.16	0.70916	67.12	58

FD(84) is a sample of the porphyritic granitic phase of the Ruby Star Granodiorite from Farmer and DePaolo (1984).
Error represents 2 standard deviations from the mean and is based on in-run statistics.
Analysis of the La Jolla standard gave values of $^{143}Nd/^{144}Nd$=0.511866±14.
Analysis of NBS-987 yielded values of $^{87}Sr/^{86}Sr$=0.710241±46.

Table 4. INAA of trace-element compositions. Values in ppm unless otherwise noted.

	DIORITE		ANDESITE						
	D-MR2-2	D-MR2-3	KD-GR2-7	KDR-GR2-9	KDGR-4	KD-GR2-5	6-81-2	KD-GR2-1	% error
Na %	3.00	2.97	3.66	3.25	2.83	3.07	2.57	3.48	1.0
K %	2.81	2.97	3.03	3.15	3.04	2.99	2.49	3.54	1.9
Ca %	3.64	3.53	2.04	2.45	2.70	3.45	2.80	1.57	3.0
Sc	8.98	8.52	6.93	6.92	6.91	6.74	6.64	6.35	1.0
Mn					764.00		769.80	n.d.	1.2
Fe %	4.30	4.10	3.92	4.43	3.90	3.78	3.70	3.77	1.0
Co	14.79	13.78	14.47	15.51	14.34	13.61	13.54	10.65	1.0
Ni	4.86	2.28	8.40	3.17	14.66	12.49	13.45	8.21	26.7
Cu **		25.00			37.00	32.00	25.00	15.00	
Zn	82.48	73.30	79.50	129.90	78.78	76.12	74.34	66.34	2.3
Rb	113.70	116.10	98.11	115.90	111.80	101.50	95.09	114.80	1.0
Sr	642.31	615.67	853.72	926.37	503.79	656.40	457.60	615.87	2.4
Zr	236.36	221.13	178.26	205.23	170.35	169.27	161.95	171.53	2.2
Cs	3.30	3.63	2.48	4.73	7.92	12.15	14.37	5.80	1.6
Ba	978.59	1002.21	1016.56	1331.64	1145.64	1004.62	952.26	1016.64	1.4
La	38.57	38.30	32.36	33.99	32.05	30.47	30.08	32.52	1.0
Ce	71.00	70.04	59.03	61.87	57.97	55.03	58.29	59.90	1.0
Nd	33.34	32.12	28.55	30.09	28.67	26.77	27.92	27.95	1.5
Sm	5.68	5.54	4.79	5.01	5.02	4.57	4.80	4.68	3.4
Eu	1.400	1.355	1.284	1.396	1.33	1.236	1.26	1.26	1.2
Tb	0.62	0.59	0.45	0.52	0.51	0.46	0.48	0.44	4.2
Tm	0.29	0.26	0.20	0.23		0.17		0.17	
Yb	1.961	1.943	1.253	1.358	1.26	1.210	1.21	1.18	2.5
Lu	0.345	0.327	0.208	0.222	0.211	0.202	0.203	0.197	2.50
Hf	5.66	5.46	4.36	4.76	4.77	4.11	4.43	4.45	3.0
Ta	0.70	0.64	0.62	0.53	0.557	0.56	0.521	0.62	2.8
Th	12.60	12.12	6.95	6.33	6.23	6.55	6.04	7.17	1.0
U	3.57	3.46	1.94	1.57	1.61	1.69	1.53	1.57	2.0
K/Rb	247.14	255.81	308.84	271.79	271.91	294.58	261.86	308.36	
K/Ba	28.71	29.63	29.81	23.65	26.54	29.76	26.15	34.82	

** Cu determined by Inductively Coupled Plasma (ICP) analysis.

Table 4. (cont.)

	GRANODIORITE						LATE-STAGE BODIES		
	RS-MR-5	RSMR3-6	RSMR-8	RSMR3-2	RSMR3-5	RSMR3-8	QL-MR-7	TWB-PA	QL-85-1
Na %	2.89	3.04	3.19	2.95	3.07	3.02	3.03	2.91	2.74
K %	3.08	3.25	2.93	3.09	3.17	3.28	3.56	3.08	2.15
Ca %	2.38	1.94	1.99	1.71	1.89	1.50	1.57	1.49	0.96
Sc	5.03	3.87	3.71	3.56	3.47	3.28	3.83	3.47	3.29
Mn	395.20	283.30	370.00	151.80	345.80	316.00			
Fe %	2.36	2.22	2.19	2.05	2.01	1.59	2.02	1.37	1.26
Co	8.49	5.90	6.29	3.79	5.85	4.23	4.79	3.68	3.64
Ni	11.87	8.27	6.38	7.38	9.47	7.08	6.01	3.49	3.46
Cu **	<5.	120.00				80.00			
Zn	42.09	31.52	41.40	27.32	39.30	33.23	31.94	39.61	25.70
Rb	146.45	164.70	142.30	163.05	149.50	163.75	160.70	154.70	247.70
Sr	448.37	507.21	528.35	468.75	511.48	420.16	479.11	481.80	391.17
Zr	132.25	168.14	175.04	166.66	161.01	151.62	184.96	166.07	181.62
Cs	3.97	3.53	3.28	3.27	3.37	3.66	3.81	2.28	3.18
Ba	878.59	1029.38	891.64	1154.19	1090.93	1138.03	1350.19	1097.37	1523.79
La	34.21	30.99	31.38	30.11	30.28	29.00	37.65	34.70	31.95
Ce	55.32	55.31	55.94	56.50	52.85	51.55	67.15	61.34	56.21
Nd	21.31	24.16	24.08	24.76	22.33	19.39	28.21	24.02	23.37
Sm	3.64	3.94	3.95	3.89	3.70	3.30	4.28	3.77	3.76
Eu	0.837	0.906	0.924	0.874	0.88	0.724	0.97	0.85	0.94
Tb	0.331	0.363	0.347	0.327	0.36	0.306	0.38	0.35	0.35
Tm							0.20	0.18	0.12
Yb	0.98	1.16	1.01	0.93	0.94	1.05	1.26	1.24	0.97
Lu	0.172	0.202	0.176	0.160	0.16	0.185	0.22	0.19	0.15
Hf	4.07	4.78	4.98	4.68	4.50	4.41	4.92	4.78	5.51
Ta	0.735	0.804	0.679	0.678	0.63	0.679	0.72	0.68	0.68
Th	21.10	10.99	11.86	12.12	12.75	12.11	13.87	9.29	11.93
U	6.07	2.76	2.51	3.61	2.53	4.11	3.57	2.88	5.52
K/Rb	210.31	197.33	205.90	189.51	211.71	200.31	221.53	198.84	86.80
K/Ba	35.06	31.57	32.86	26.77	29.01	28.82	26.37	28.03	14.11

** Cu determined by Inductively Coupled Plasma (ICP) analysis.

Table 4. (cont.)

	APLITES AND RHYOLITES						ALTERED SAMPLES			
	RSMR-6	RSMR-4	KDR-GR-7	KR-MR2-4	KR-3	KR-2	RSMR3-3	RS-MR3-4	RS-SM-1	RS-SM-10
Na %	2.18	2.73	2.57	2.23	3.89	3.38	2.72	1.72	2.91	3.10
K %	4.57	4.38	4.55	3.45	1.47	2.20	6.73	10.47	2.32	3.65
Ca %	0.50	1.17	0.52	1.62	0.63	0.47	1.33	0.41	2.10	1.60
Sc	0.83	2.30	1.60	3.36	3.94	3.54	4.74	4.34	5.52	3.80
Mn	24.61	161.40		0.00			228.30			
Fe %	0.47	1.31	0.66	1.82	0.59	0.66	1.15	0.94	2.65	1.55
Co	0.80	4.09	1.00	6.28	0.49	0.66	2.91	2.02	8.42	3.49
Ni	5.25	7.39	2.90	7.62	1.85	4.09	6.33	6.55	8.50	9.29
Cu **				5.00					205.00	1150.00
Zn	4.59	23.93	13.89	42.12	34.46	24.28	30.51	21.61	35.35	30.55
Rb	190.40	211.70	144.10	153.85	116.10	113.20	361.10	430.20	149.80	158.20
Sr	63.17	350.03	214.63	277.25	76.18	183.09	445.59	380.72	487.21	485.95
Zr	65.03	190.63	95.62	140.07	85.96	85.50	179.34	201.48	151.51	169.01
Cs	2.70	4.65	4.16	9.30	2.91	2.83	7.67	6.14	5.72	3.51
Ba	202.64	1501.84	789.29	1723.18	69.87	259.25	1146.21	1513.56	964.48	1444.67
La	23.85	49.09	24.77	37.15	13.57	15.91	39.99	14.51	34.52	27.38
Ce	28.67	82.57	41.12	62.12	29.69	29.07	72.33	24.72	57.51	46.73
Nd	6.60	28.88	15.56	24.25	15.52	15.51	28.98	9.44	24.10	18.05
Sm	0.93	3.87	2.32	3.72	4.05	3.57	3.78	1.72	3.77	2.84
Eu	0.179	0.835	0.489	0.857	0.35	0.38	0.783	0.74	0.925	0.819
Tb	0.071	0.218	0.21	0.35	0.74	0.55	0.277	0.17	0.34	0.24
Tm			0.11	0.18	0.52	0.37		0.10	0.16	0.13
Yb	0.41	0.475	0.816	1.491	3.56	2.86	0.59	0.74	1.064	0.950
Lu	0.086	0.087	0.147	0.264	0.55	0.45	0.117	0.14	0.183	0.174
Hf	2.50	5.51	3.20	4.00	4.80	4.16	5.13	5.37	4.19	4.48
Ta	0.478	0.749	0.67	0.95	1.84	1.47	0.594	1.39	0.84	0.68
Th	30.94	18.59	7.75	13.02	22.85	19.00	13.41	17.43	18.22	15.69
U	4.73	5.15	2.68	5.81	10.21	7.05	3.50	6.33	4.04	5.84
K/Rb	240.02	206.90	315.75	224.24	126.72	193.98	186.37	243.38	154.87	230.72
K/Ba	225.53	29.16	57.65	20.02	210.55	84.70	58.72	69.17	24.05	25.27

** Cu determined by Inductively Coupled Plasma (ICP) analysis.

rather than a true partition coefficient, but it does allow one to evaluate the relative preference in the minerals for one element over another.

Also, as Figure 3 shows, the values for the mineral/whole rock ratios have the same shape as true partition coefficients. The comparison is based on both experimental studies (Drake, 1975, Drake and Weill, 1975, Nicholls and Harris, 1980) and phenocryst/glass determinations (Arth, 1976). For titanite, no experimental data are available and the comparison is based on other mineral/whole rock determinations (Fourcade and Allegre, 1981, Gromet and Silver, 1983). The similarity between partition coefficients and mineral/whole rock ratios implies that the denominator for each is similar, that is, the whole rock values are representative of liquid compositions (Gromet and Silver, 1983). The only substantial discrepancy in this general statement is the values of La and Ce in the hornblende; these two elements usually have smaller partition coefficients than the remainder of the REE.

That the whole-rock concentrations are representative of liquid rather than cumulate concentrations is also supported by the modal and normative compositions of the granodiorite. On a quartz-albite-orthoclase ternary diagram (Figure 4), the normative compositions cluster around the minimum melt composition for 4 kilobars water pressure (Winkler, 1979),

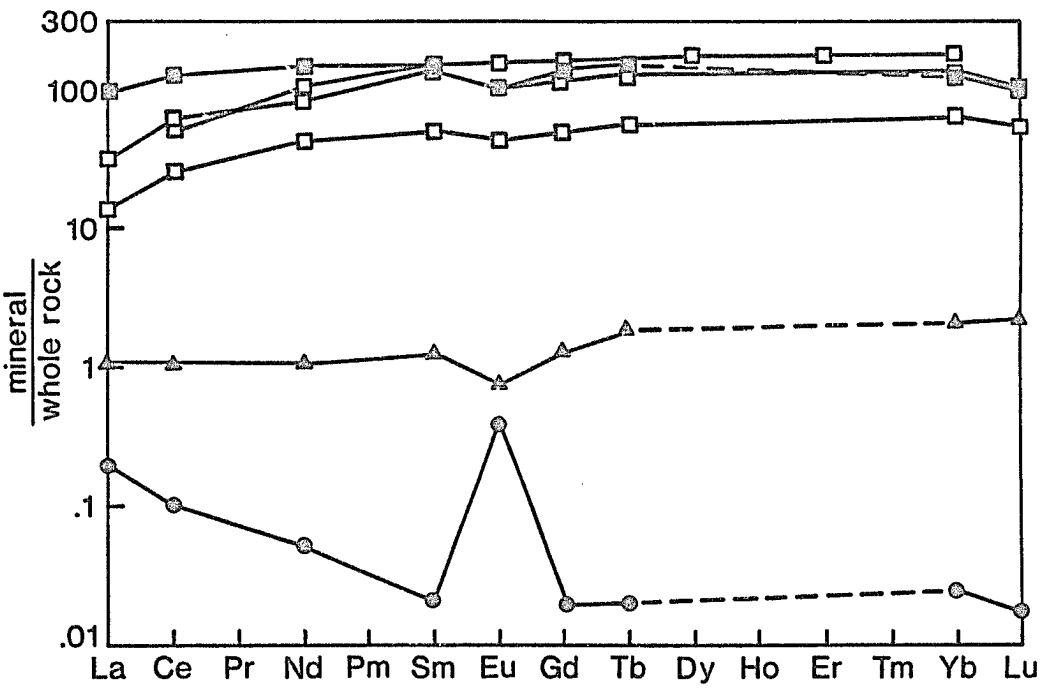

Figure 3a. Mineral concentration/whole rock concentration for mineral separates from the granodiorite. Circles represent plagioclase; triangles, hornblende;and squares, titanite. Filled squares are from this study; open symbols from Gromet and Silver (1983) and Fourcade and Allegre (1981).

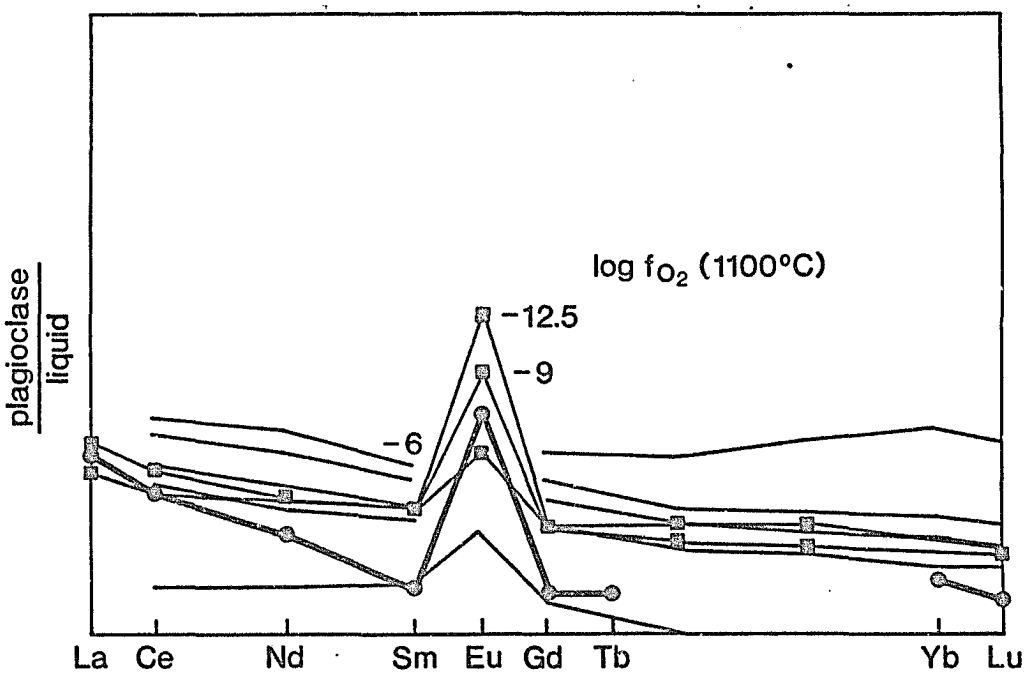

Figure 3b. Comparison of mineral concentration/whole rock concentration and published partition coefficients for the mineral plagioclase. Heavy line from this study, light lines with symbols from Drake (1975) and Drake and Weill (1975). Light lines without symbols from Arth (1976).

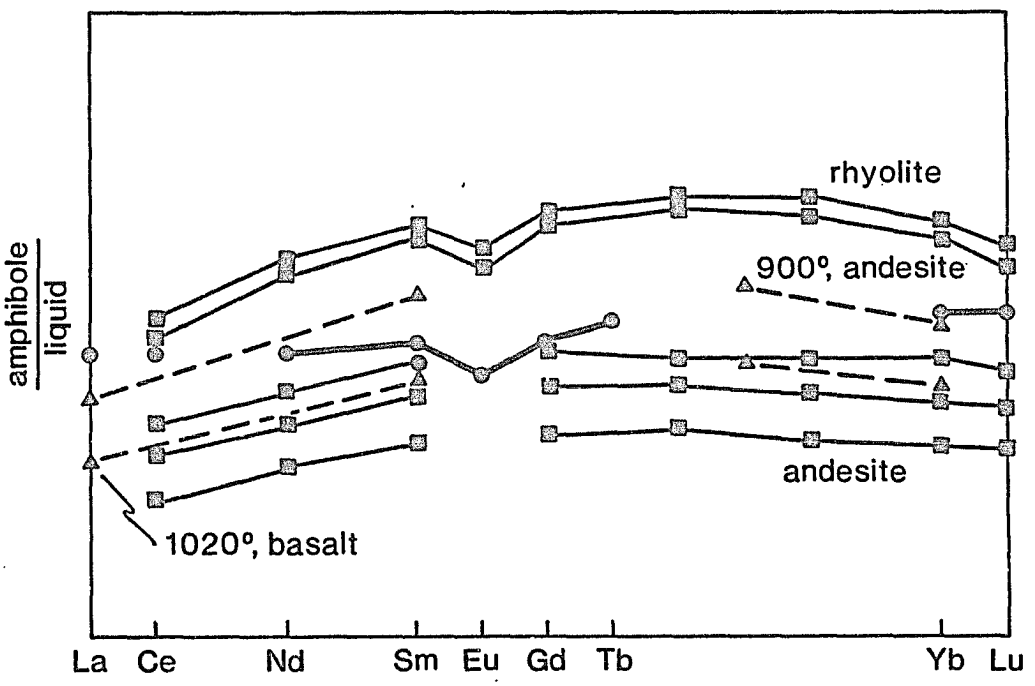

Figure 3c. Comparison of mineral concentration/whole rock concentration and published partition coefficients for the mineral amphibole. Heavy line from this study. Light lines with squares from Arth (1976) for rhyolite and andesite. Light lines with triangles from Nicholls and Harris (1980).

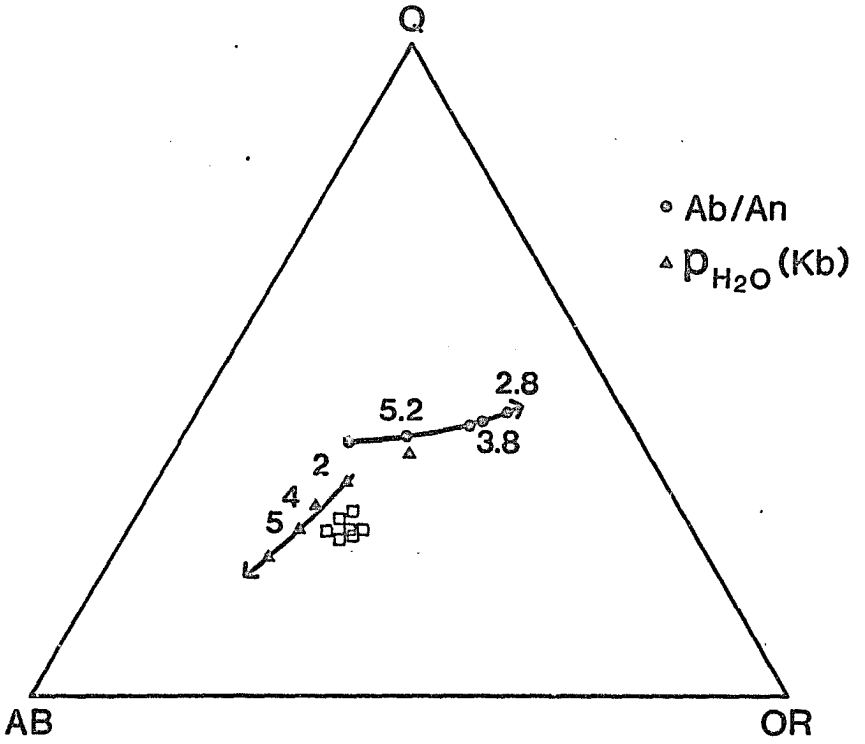

Figure 4. Quartz-albite-orthoclase diagram of the normative compositions of the Ruby Star Granodiorite. Trends for increasing water pressure and decreasing Ab/An content of the feldspar component for Winkler (1979).

and are displaced from the curve in the direction expected by consideration of the effect of anorthite in the quarternary system.

Isotopic Ratios

Isotopic values for Nd and Sr vary sympathetically (Figure 5 and see Table 3, p. 20), with the oldest and least evolved rock characterized by an ε_{Nd} of -4.3 and a $^{87}Sr/^{86}Sr$ of .7069 and the youngest and most evolved, with an ε_{Nd} of -8.6 and a $^{87}Sr/^{86}Sr$ of .7096. Epsilon strontium values were calculated from initial strontium ratios according to equations found in Farmer and DePaolo (1984).

Trace-Element Patterns

Figure 6 plots ε_{Nd} against SiO_2 and selected trace elements. The figure shows that ε_{Nd} decreases with increasing SiO_2 or progressive differentiation for the main rock units of the suite -- the andesite, granodiorite, and late-stage bodies. Figures 7 and 8 compare the trace element patterns for the three main rock units of the Sierrita system. They indicate that variations in most trace elements reveal the same trends as the three elements represented in Figure 6. Elements are related by continuous changes, with few reversals, in the direction expected by differentiation. Concentrations of the compatible elements (the transition element and

Figure 5. Epsilon Nd versus epsilon Sr. Numbers along the top of the graph are $^{87}Sr/^{86}Sr_0$. Ages of the units are plotted on the right ordinate. Circle, andesite; squares, granodiorite; open triangle, late-stage dike; star, quartz diorite; closed triangle, Red Boy Rhyolite. With the exception of the diorite and the rhyolite, the samples represent a continuous trend of increasing crustal character with respect to decreasing age from the andesite through the granodiorite to the late-stage bodies.

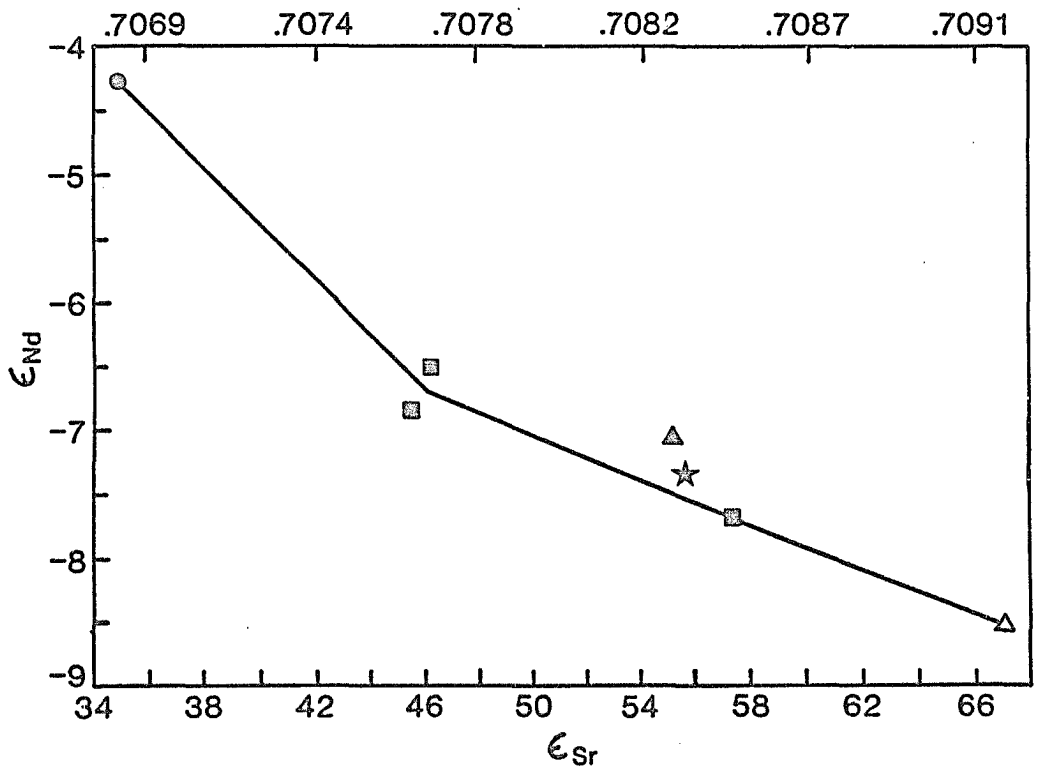

Figure 5. Epsilon Sr versus epsilon ND for samples from Sierrita.

Figure 6. Epsilon Nd versus various indices of differentiation. Decreasing ε_{Nd} is correlated to increasing Rb (dotted line) and SiO_2 (solid line) and decreasing Sc (dashed line) for the same progression of samples -- andesite, granodiorite, granite -- as in Figure 5 (see p. 30). These trends imply that the samples are related by coupled assimilation and differentiation.

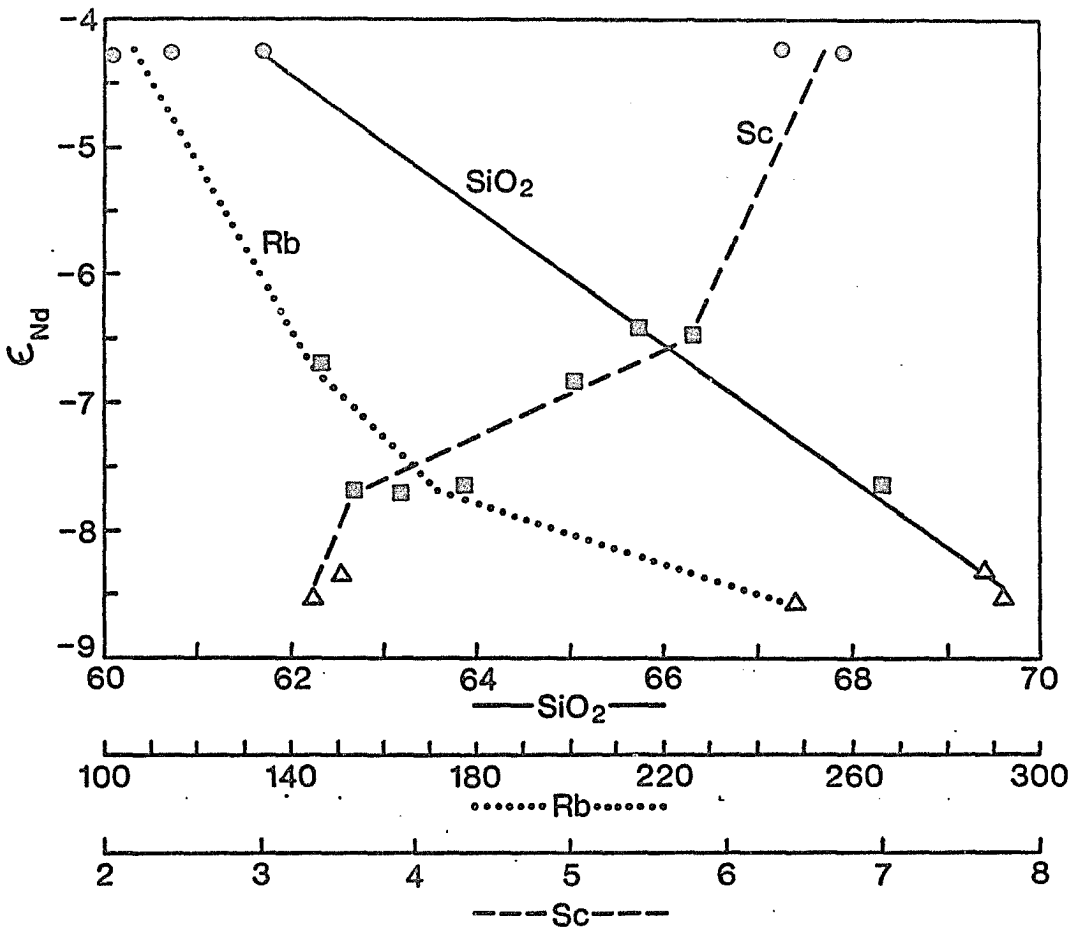

Figure 6. Epsilon Nd versus elemental concentrations.

Figure 7. Elemental concentrations of the rare-earth elements. Chondrite normalization values from Anders and Ebihara (1982). 7a. The band of vertical hachuring encloses analyses of andesites. The diagonal hachuring encloses granodiorite samples. Analyzed elements are represented by filled circles and squares, respectively. The younger granodiorite is depleted in most elements relative to the older andesite, and the patterns pivot on La and Ce. Note also the limited Eu anomaly and the concavity in the HREE. These observations imply that pyroxenes or amphibole combined with plagioclase governed melting and crystallization. 7b. Diagonal hachuring are fields from 7a. The three samples of porphyry bodies and dikes are shown as open triangles. These late-stage bodies are similar to the granodiorite except they are enriched in the HREE.

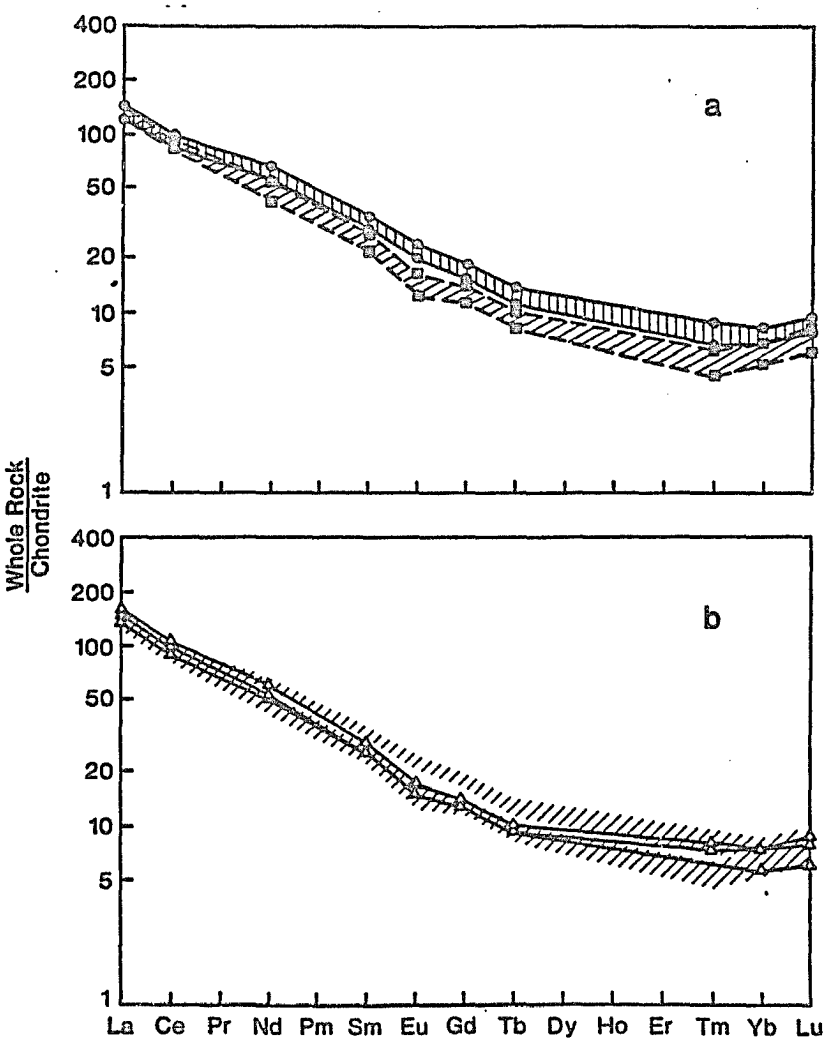

Figure 7. Rare-earth element concentrations for whole-rock samples.

Figure 8. Enrichment factors for the granodiorite relative to the andesite. An average of the six andesite samples was used as the basis of comparison. X's represent actual ratio values. Only Rb, Ta, Th, and U are incompatible with respect to all granodiorite samples. Transition elements are the most compatible in the system followed by the middle REE.

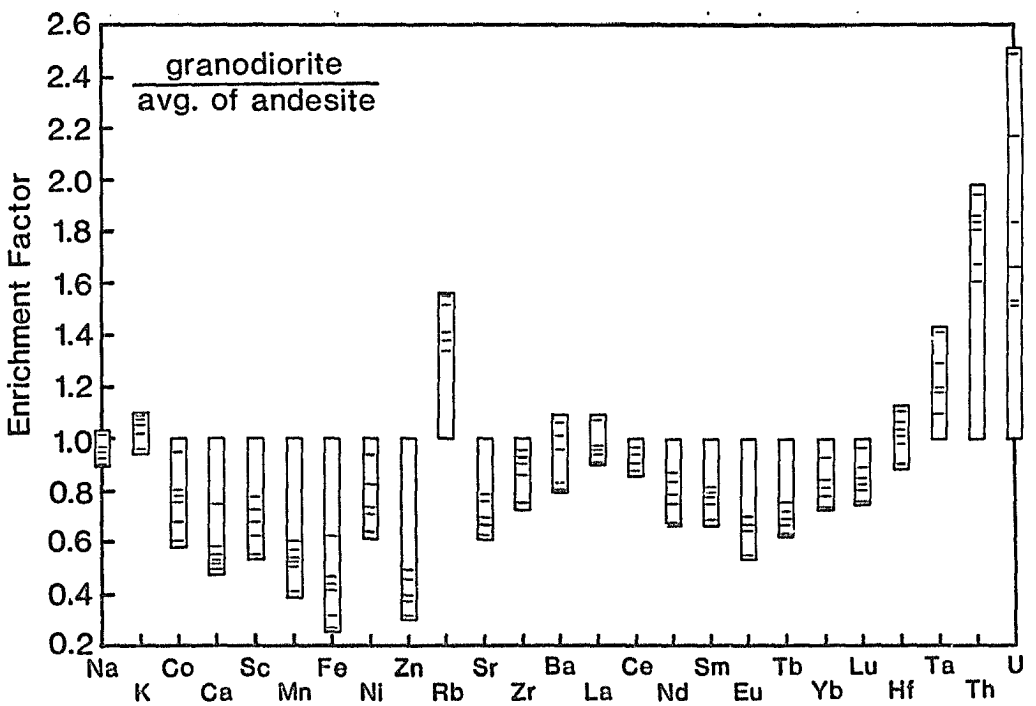

Figure 8. Concentrations of incompatible and compatible elements.

the REE) decrease while concentrations of the incompatible elements (Rb, Ta, Rh, U) increase.

The REE are considered compatible elements in this series because early crystallization is dominated by plagioclase and hornblende in approximately subequal amounts, and hornblende has partition coefficients for the middle and heavy REE of 2 and greater. Further, the REE pattern pivots on La and Ce as would be predicted by the lower K_d (hornblende) for these LREE. Titanite is also an early phase and it has partition coefficients for the REE which range from 50 to 150 (see Table 2, p. 19 and Fourcade and Allegre, 1981, Gromet and Silver, 1983). However, its importance in producing the patterns must be qualified by the observation that Ta, which has a larger partition coefficient into titanite than do the rare earth elements (Table 2), increases from the andesite to the granodiorite.

CHAPTER 4

INTERPRETATION

The negative epsilon values for Nd and the positive values for Sr suggest that no rocks in the sequence were derived from pure mantle melts. The absolute values and the covariance of the isotopes suggest that the lithologies represent mixtures of crustal and mantle components. The chemical trends towards differentiation, when combined with the isotopic trends and the understanding that the suite was generated during a period thought to have been one of active subduction in southern Arizona, suggest that a reasonable model for the igneous process is progressive assimilation of crust by originally mafic, mantle-derived magmas, a model which has been proposed for igneous systems in other areas of similar tectonic setting (Taylor, 1980, DePaolo, 1981a, Ben Othman et al., 1984, Grove et al, 1985).

Consanguinity of the Rock Units

Deferring for the moment the question of the diorite and rhyolite, which are anomalous with respect to age and chemistry on diagrams as shown in Figures 5-8 (see pp. 30-33), the question which must be addressed is whether the different lithologies are directly related to each other, that is,

are consanguinous, or whether they are simply representative of similar processes which operated in the area through time. Emplacement of the different bodies represents a series of events separated in time. Is it reasonable that the rocks were related at depth by a continuous process acting on a single large volume of material? The duration of igneous activity, 5 to 10 million years, is sufficiently long to raise doubt among some readers as to the reasonableness of a close genetic link between the various units.

Certainly there is ample proof of a spatial and temporal coherence in the suite. The phenocryst-rich nature of the andesite implies that it is found close to its vent, and thus that all magmas must have passed through the same vertical section of crust. The temporal coherence of the suite is in the observation, reviewed in the section on geochronology, that these units represent a continuous episode of magmatism, and one which is separated from other episodes by 80 m.y. in the Jurassic and 40 m.y. in the Tertiary.

Further, the Laramide in southeastern Arizona was a time of intense igneous activity which, it has been postulated, was related to high subduction rates. Other porphyry-related igneous suites show a duration similar to that of Sierrita, and the duration is coupled to an evolution of chemical compositions like that at Sierrita. For example,

the deposit at Ray, Arizona, is associated with rocks of diorite through granite in composition and ages of 71-59 million years (Banks et al., 1972). The deposit at Christmas also shows the same chemical variation and a duration of activity of 14 million years, from 76-62 m.y. ago (Koski and Cook, 1982). Given these supporting examples, perhaps modern analogs of smaller systems (and slower subduction rates ?) are not appropriate models.

The precise nature of the relationships becomes a question of a complexity of the geometry of the magma chambers that existed during the ten million year period of Laramide magmatism. Did small chambers become isolated from each other and undergo separate assimilation and crystallization? Certainly there is geochemical evidence for local complexities in magma chamber geometry. However, chemical evidence for isolated chambers relies on reversals or noncontinuities in some appropriate chemical index, and chemical changes at Sierrita are continuous and without reversals (compare Figures 5-8, pp. 30-33). Lack of a more definitive knowledge of the dynamics of magma systems however makes it necessary to remind the reader that the model, with its implications of a continuous process, is only one possible hypothesis, albeit reasonable. The following discussions and models will explore the consequences of the hypothesis.

The two points in Figure 5 (see p. 30) anomalous with respect to age are the quartz diorite and the Red Boy Rhyolite. Both are similar to the granodiorite in their isotopic composition although they are older than it. The similarity suggests that these units represent a process similar to that which created the other units, but which occurred at an earlier time.

More detailed studies of these units would be necessary to determine the nature of the process which was responsible and its relation to the main series of rocks. For instance, in an isotopic study of a mafic-felsic complex in the Pyrenees, Ben Othman et al., (1984), report ε_{Nd} for a hornblende peridotite which is more crustal in character than the other mafic rocks and similar to the granodiorite in their area. They interpret the sample as either re-equilibrated because of its low Nd content (not a tenable explanation for the diorite of Sierrita because it has the highest Nd content of any rock in the area) or simply as a crustal xenolith. The latter interpretation seems reasonable for the diorite of Sierrita, especially given its intrusive contacts (see Figure 1, p. 8): along its northern contact it appears to be intrusive into the granodiorite, although the granodiorite is thought to be five million years younger than it. Cooper (1960) also discusses the anomalous geologic relations involving this rock.

The origin of the rhyolite is more problematical. It may represent crustal melting, without little mixing, during the initial invasion of the crust by mantle-derived magmas. Interpretation is made difficult by the extreme variation in chemical compositions of the few samples analyzed (see Table 1, pp. 10-12 and Table 4, pp. 21-23). A more thorough analysis of the chemical trends is underway (Anthony and Titley, in prep.)

It is important to emphasize that major and trace element patterns alone would allow interpretation of the sequence as related solely by differentiation. As was discussed above, this interpretation is consistent with the data presented in Figures 7 and 8 (see pp. 32-33), which show that compatible elements decrease and incompatible elements increase with respect to decreasing age. Incorporation and evaluation of the isotopic data allow the added dimension of assimilation to be considered. There exists the potential that other suites which have traditionally been interpreted as derived wholly by fractional crystallization will be more accurately modelled by combined assimilation and crystallization.

Oxidation State of the Magmas

Further evidence for the involvement of crust in the generation of the magmas is that of the redox conditions of the rocks. Three different petrological characteristics

of the suite indicate that the magmas were oxidizing. First, ilmenite is not observed in any of the samples , and beginning with at least the andesite, there is phenocrystic, early titanite coexisting with amphibole and plagioclase. The stability limits for this assemblage (Noyes et al, 1983b) are shown in Figure 9. Second, there is no Eu anomaly in the earliest magmas (see Figure 7, p. 32). This lack of an anomaly implies that the Eu^{2+}/Eu^{3+} of the source materials must have been quite low.

The third indicator is found in the oxidation state of the magmas as determined by the compositions of biotite coexisting with potassium feldspar, magnetite, and quartz (Hess, in prep., Hess et al, in prep.). For the reaction:

$$KFe_3AlSi_3O_{10}(OH)_2 \text{ (annite)} + 1/2\ O_2 =$$
$$KAlSi_3O_8(kf) + Fe_3O_4(mt) + H_2O,$$

the equilibrium relation (Wones, 1972) is:

$$1/2 \log f_{O_2} =$$
$$7409/T(K) + 4.25 - \log f_{H_2O} + \log a_{ann} \log a_{kf} - \log a_{mt}.$$

We use:

$$a_{ann} = X^{VI}_{Fe^{2+}}/6 \cdot X_{OH}/4,$$
$$a_{mt} = 1, \text{ and } a_{kf} = 0.6,$$

Figure 9. Oxygen fugacity versus temperature. TMQA represents the equilibrium between titanite-magnetite-quartz-amphibole from Noyes et al. (1983b). BKM indicates oxygen fugacities of the Sierrita magma calculated from potassium feldspar-magnetite-biotite equilibria (Hess et al., in prep.). Calculations imply that oxygen fugacities were within a few log units of HM at magmatic temperatures (i.e., 600-700° C). The uniformity of biotite compositions implies that the magma crystallized at a constant oxygen fugacity, and therefore that it was intrinsically oxidized and resulted from melting of oxidized, crustal rocks.

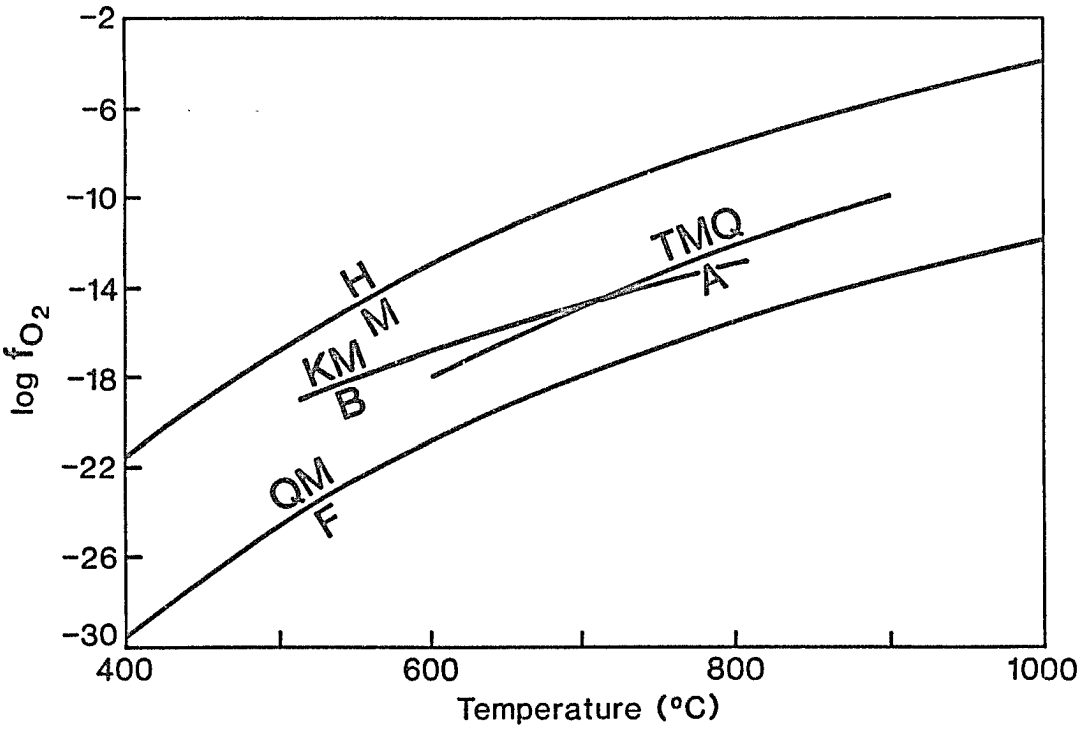

Figure 9. Oxygen fugacity versus temperature.

according to the convention of Noyes et al. (1983b) and values for the fugacity of water from Burnham et al. (1972).

Table 5 summarizes the data on biotite compositions for both equigranular and porphyritic phases of the granodiorite and the oxygen fugacities calculated using the expressions above. Figure 9 (see p. 41) shows the oxidation trends along with well-known iron oxide buffers. Precise temperatures of crystallization are not known so the oxidation trends are plotted as trajectories for the range of temperatures reasonable for the solidus in granodiorite-granite systems.

Oxidation trends for the various samples are superposed on each other because of the very limited range of Fe^{2+} observed observed throughout the granodiorite. The range is from $X^{Fe2+}(VI)$ = Ø.25 - Ø.29, which corresponds to less than half a log unit of difference in oxygen fugacity. The gentle slope for the oxidation trends is essentially that of the biotite equilibrium. This observation can be explained by buffering of the system by the ferromagnesian minerals, a process which is inefficient because two moles of annite are needed for each mole of O_2 (Mueller, 1971), or by some external buffer. Mueller (1971) suggests that H_2O would be a good buffer in water-rich magmas, and can thus explain the trends in iron-enrichment observed in calc-alkaline rocks.

Table 5. Compositions of biotites from the Ruby Star Granodiorite

	RS-MR3-6	RS-MR-5	RS-MR3-8	RS-MR-8
SiO2	37.14	37.68	37.98	37.57
Al2O3	15.27	13.32	13.8	14.31
TiO2	3.05	3.9	3.12	3.13
FeO(T)	17.36	17.35	16.07	16.8
MgO	13.19	13.32	13.89	13.98
CaO	0.01	0.01	0	0
MnO	0.36	0.51	0.66	0.55
Na2O	0.07	0.6	0.1	0.08
K2O	9.46	9.46	9.41	9.19
F	0.6	0.3	0.96	0.43
Cl	0.04	0.02	0.03	0.02
Total	96.55	95.93	96.02	96.06
Si	5.573	5.622	5.722	5.608
Al	2.427	2.362	2.278	2.392
Fe(IV)	0	0.16	0	0
Al(VI)	0.105	0	0.163	0.139
Fe3+(VI)	0.402	0.447	0.414	0.639
Ti	0.33	0.401	0.346	0.324
Mg	2.915	3.096	3.025	2.943
Fe2+(VI)	1.712	1.642	1.558	1.491
Mn	0.401	0.057	0.08	0.072
Ca	0.206	0.007	0.003	0.006
Na	0.009	0.021	0.024	0.016
K	1.833	1.81	1.806	1.722
F	0.2832	0.1428	0.4438	0.2033
Cl	0.0101	0.0051	0.0101	0.0076
log fO2 (500)	-19.39	-19.28	-19.14	-19.03
log fO2 (600)	-16.92	-16.81	-16.67	-16.56
log fO2 (700)	-15.01	-14.9	-14.76	-14.65

Microprobe analyses by N.Hess (in prep.).
Fe2+/Fe3+ determinations by Mossbauer spectroscopy (M.D. Dyar, personal communication, 1985).

Water as a buffer is an attractive hypothesis for the granodiorite of Sierrita, because the magmas were known to have been very water-rich, and, as can be seen in Figure 9 (see p. 41), they were also quite oxidizing. The oxidation trends approach the hematite-magnetite boundary at the solidus temperatures for granite. Because changes in the oxidation state of magmas are sluggish, we interpret this high oxidation to be intrinsic to the materials which melted, and thus to be indicative of generation of melt from crustal rather than mantle materials.

Isotopic and Petrologic Characteristics of the Crust

A question addressed in this section is whether the rocks with the most negative ε_{Nd}, the late-stage dikes and porphyry bodies with $\varepsilon_{Nd} = 8.5$, are wholly crustal in character, or whether they retain some mantle isotopic signature. Figure 10 represents the epsilon values which result from the melting of materials with various Sm/Nd ratios. The particular values found in the figure were calculated using the following assumptions: the protolith which melted was 1.7 Ga old and had been generated itself by melting of a rock with $\varepsilon_{Nd} = +5$, a value appropriate for Proterozoic depleted mantle (Patchett and Bridgwater, 1984). Melting of this protolith occurred at 65 million years ago. These ages represent the approximate basement age and age of Laramide igneous activity for the area.

Figure 1Ø. Epsilon Nd versus $^{147}Sm/^{144}Nd$ ratios. Sample designations are: nas, North American Shale; grwy, graywacke; crb, Columbia River Basalt; aleut, Aleutian basalts; chur, chondritic undepleted reservoir; and morbg, MORB glass. All values from Goldstein et al. (1984). The ε_{Nd} values are calculated for the various Sm/Nd ratios assuming a 1.7 Ga material which melted 65 m.y. ago. A $^{147}Sm/^{144}Nd$ of approximately Ø.135 would be required to generate a material with an ε_{Nd} of -8.5. This value is substantially more Sm-rich than most supracrustal materials, i.e., nas, granite, grwy, however, it may well be typical of mafic (lower ?) crust.

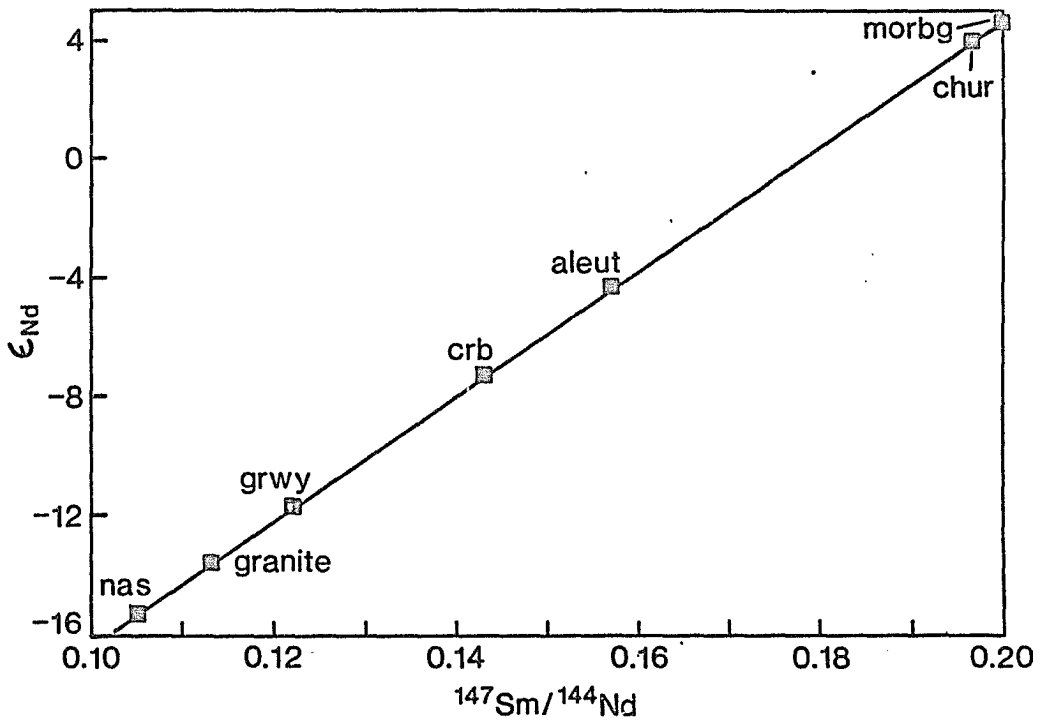

Figure 1Ø. Epsilon ND versus $^{147}Sm/^{144}Nd$ for various lithologies.

It may be seen in Figure 10 (see p. 45) that, with these age constraints, a rock with a Sm/Nd ratio of approximately 0.135 would yield a melt with a ε_{Nd} of -8.5. This Sm/Nd ratio is higher than the typical ratios for supracrustal materials such as shales, graywackes and granites, average values for which are shown in Figure 10, and implies melting of a more mafic material.

An intermediate to mafic parent is consistent with petrologic and chemical characteristics of the Sierrita suite which suggest that the source was an amphibolite. The evidence includes:

1) The intrinsic oxygen and water fugacities of the magma. As discussed by Burnham (1981) only amphibole-rich rocks such as amphibolites have the requisite water content to generate large amounts of partial melt with elevated water contents. The high water content of the Sierrita magmas is indicated by the presence of amphibole. To stabilize amphibole in granodiorite melts a minimum of approximately 4 weight percent water is required (Naney, 1983). In the samples from Sierrita, amphibole is an early, although not necessarily a liquidus phase, and thus the magmas must have been water-rich at their inception rather than having developed an elevated water content during the latter stages of their evolution. In addition, arguments for suggesting that water served as an oxidant and buffer

for the high oxidation states of the magmas have been outlined above.

A large degree of melting is indicated by the longevity of the magmatic event at Sierrita, the volume of co-genetic magma, and the limited enrichment of incompatible elements. Elements such as Rb, Cs, and Ba are enriched approximately 2 to 3 times over values for crustal mafic rocks such as continental tholeiites; these enrichment factors imply 30 to 50 percent melting.

2) The mineral composition of the source region. The same shape for the REE pattern is exhibited by all rock types, even the least differentiated andesite (see Figure 7, p. 32); the shape is characterized by upward concavity, especially for the heavy rare-earth elements (HREE), and a very small europium anomaly. The small Eu anomaly suggests that some mineral with a small preference for Eu^{2+}, such as pyroxene, amphibole, or titanite, was in equilibrium with the melt along with plagioclase (Noyes et al., 1983a). The argument for the presence of one of the mafic minerals or titanite is strengthened by the concavity of the REE pattern, because these minerals have a preference for the middle REE relative to La, Ce, and Yb (see Figure 3, pp. 25-27).

The proportions of plagioclase and amphibole required to obtain a smooth trend in the rare earth elements is

a function of the oxygen fugacity of the magma, because of the partition coefficient for Eu in plagioclase is dependent on Eu^{2+}/Eu^{3+}. There exist very little data on the variation of the partition coefficient with respect to oxygen fugacity; however, analyses performed on the mineral separates for this suite (see Table 2, p. 19) suggest that K_d(hbl) = Ø.7 and K_d(plag) = Ø.4. Calculations based on these values require that the melt be in equilibrium with a material of approximately forty percent amphibole and sixty percent plagioclse to generate the observed Eu value. This mineral composition is consistent with melting of an intermediate to mafic amphibolite rather than a felsic gneiss which has a smaller modal fraction of the hydrous minerals. Ratios of incompatible elements provided additional evidence that the source was not gneissic: constant ratios of K/Rb and K/Ba (see Table 4, pp. 21-23) in the suite indicate that during melting the magma was not buffered by a potassium-bearing mineral, such as biotite or potassium feldspar (Hanson, 1978).

A more precise determination of the lithologic nature of the source materials is difficult because it is not known whether the melt was in equilibrium with a minimum-melting or initial composition of a mafic source or the mafic residue from more extensive melting of an intermediate source.

A number of other observations may be brought to bear on the question of the source materials. For another porphyry system, Silverbell, which is 50 miles north of Sierrita, the lead isotopes have $^{206}Pb/^{204}Pb$ = 17.96-18.5, $^{207}Pb/^{204}Pb$ = 15.54-15.59, and $^{208}Pb/^{204}Pb$ = 38.35-38.41 (Sawyer and Zartman, 1985). These workers interpret the values as characteristic of lower rather than upper crust. Also, in a study conducted on mineralized and unmineralized metaluminous granites in the part of southeastern Arizona characterized by 1.8 to 1.65 Ga Pinal Schist (Figure 11), no epsilon Nd value more negative than -8.6 is reported (Farmer and DePaolo, 1984). Only two-mica granites within the area of Pinal Schist are known to have values as negative as -10 and -11. Further, porphyry copper deposits in older terranes within Arizona have epsilon Nd values (Farmer and DePaolo, 1984) appropriate to a Sm/Nd ratio between 0.13 and 0.14 for the source materials of the magmas (Figure 11).

It is noteworthy that metaluminous rocks in other orogenic regimes have maximum negative epsilon Nd values that would be consistent with melting of non-felsic sources: for example, -4.6 to -8.4 for the 280 m.y. old Querigut complex generated from 1.2 to 1.9 Ga basement (Ben Othman et al., 1984), +0.4 to -8.9 for I-type granites from Australia within 1.2 to 1.4 Ga crust (McCulloch and Chappell, 1982),

Figure 11. Map of Arizona showing distribution of Precambrian rock types. From Titley (1982a). The majority of copper deposits lie within the area characterized by 1.7 to 1.68 Ga Pinal Schist. ε_{Nd} for intrusive rocks associated with copper deposits in this area and in areas of older Precambrian are shown: ε_{Nd}=-11 for Bagdad and ε_{Nd}=-12.2 for Mineral Park. The minimum value for the 1.7 Ga terrains is greater. The shift can be interpreted as due to the difference in age rather than Sm/Nd ratio. Data from Farmer and DePaolo (1984) and this study.

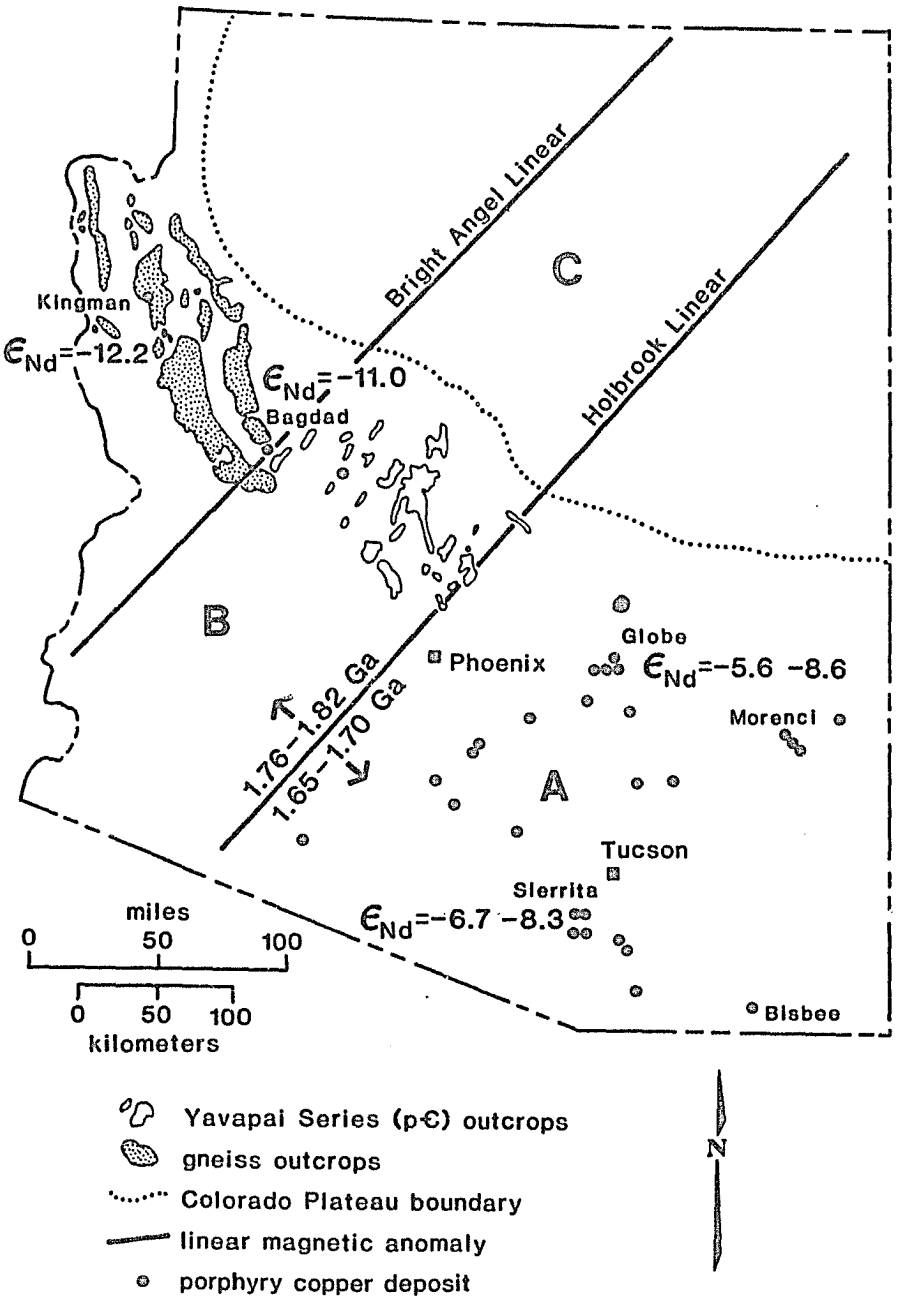

Figure 11. Map of Precambrian provinces in Arizona.

-7.6 for Sierra Nevadan samples (DePaolo, 1981b), +5 to -10 for 2.0 Ga crust in the Andes (Hawkesworth et al., 1979), and -3.2 to -9.9 for presumed 2.6 to 1.6 Ga Archean-Proterozoic crust in Scotland (Frost and O'Nions, 1985). That epsilon values demonstrate a range in so many different areas suggests that assimilation/ crystallization may be a reasonably common process (DePaolo, 1981a); the coincidence of minima may be giving us insight into the chemical composition of that part of the crust which generates metaluminous, calc-alkaline magmas.

CHAPTER 5

NUMERIC MODELLING

Given a hypothesized process, that of coupled assimilation and crystallization and knowledge of the character of the starting materials, a numeric solution of the parameters of the process, such as fraction of melt represented by the samples and percent assimilation, can be obtained using inverse techniques. The goal in using inverse methods, as in direct methods, is to solve for a set of geochemical parameters, such as distribution coefficients and initial concentrations, which are consistent with the observed trace element concentrations. The use of inverse method in trace element geochemistry was pioneered by Minster et al. (1977).

In the direct method, one assumes some knowledge of the parameters (p) of the process, and by using an operator which represents a physical process (A), transforms or maps over the parameters into data (d). The equation which represents this process is:

$$(p)\ A = d. \qquad (1)$$

In inverse methods, the data themselves are used to solve

for the parameters according to:

$$p = A^{-1} \quad (d).$$

This formalism can be applied to any process, partial or batch melting, assimilation or mixing, for which an explicit equation or operator can be expressed. There are no hidden assumptions in using inverse methods; the greatest uncertainty in their use, a problem shared equally by direct method, is whether or not the function selected accurately represents the actual physical process.

For assimilation/crystallization we use the equations developed by DePaolo (1981a) in which the rate of change of the mass (m) of an element in the magma is given by:

$$\frac{dm}{dt} = M_a C_a - M_c D C_m \qquad (2)$$

where M_a is the rate of assimilation, C_a is the concentration of the element in the assimilant, M_c is the rate of crystallization, D is the bulk distribution coefficient, and C_m is the concentration of the element in the crystallizing material.

The question which arises is whether this equation is a satisfactory representation of the actual igneous processes. It assumes bulk assimilation of the country rocks, a condition which is probably not the case (Watson,

1982), and does not allow for recharge of the magma chamber. Given that the length of time hypothesized for this suite, five to ten million years, recharge of the chamber by addition of new magma is certainly a distinct possibility. The difficulty comes in trying to model that addition, because the terms add unknowns without any additional constraints on the numeric values of those unknowns. I choose to model the simple equation with a minimum of terms as a beginning or starting point, although, as has been emphasized by many, including O'Hara (1984), consideration of additional processes can have substantial effects on the numeric solutions obtained by the modelling.

Equation 2 can be transformed into a function of f, the fraction of melt remaining, where f is the ratio of the mass of magma relative to its original mass, M_m/M_m^o. Integration of Equation 2 with respect to f and assuming a constant D and concentration of the element in the assimilant, C_a, yields:

$$\frac{C_m}{C_m^o} = f^{-Z} + \frac{r}{r-1}\,\frac{CR}{Z}\,(1-f^{-Z}) \qquad (3)$$

where r - M_a/M_c, CR - C_a/C_m, and Z is a function of both D and r according to:

$$Z = \frac{r+D-1}{r-1}$$

The concentration, C_m, of n elements in q rocks is measured and for a given value of r, the A matrix of Equation 1 is composed of equations of the type:

$$R_u = G(F_u,Z,CR)\ [R_o] \qquad u=1,\ldots,q.$$

$G(f_p,Z,CR)$ represents Equation 3, Z is the vector of weighted distribution coefficients $Z_1,\ldots,Z_n$, CR the vector of concentration ratios for the two reservoirs $CR_1,\ldots,CR_n$, and R_o is the vector of initial concentrations $c_o(1),\ldots c_o(n)$.

In order to solve the q equations, a data vector of length n x q:

$$d = [c_1(1),\ldots,c_n(q)],$$

and a model vector of length 3n + q:

$$p = [c_o,\ldots,c_o(n),Z_1,\ldots Z_n,CR_1,\ldots CR_n,F_1,\ldots,f_q]$$

is constructed.

The variable r, the ratio of assimilated to crystallized material, could be included in the equations above, however its inclusion would result in a degree of indeterminancy because different values of r can be used to transform the other variables (Minster et al., 1977). Instead, the value of r to be used in the above equations is independently determined.

Numeric Solution of r

An estimate of the numeric value of r has been made based upon the isotopic compositions of the rocks. This approach was adopted because the equation which describes changes in isotopic compositions during assimilation/crystallization has fewer interdependent variables than does the equation for trace elements. Also, because isotopes do not fractionate during melting or crystallization, the values which characterize the mantle and crustal reservoirs are better understood. The equation is (DePaolo, 1981a):

$$\varepsilon_m = \varepsilon_a + \frac{(\varepsilon_m^o - \varepsilon_a)C_m^o}{C_m f^{-Z}}$$

where ε_m is for the magma, ε_a is for the assimilant, and the other symbols are as above.

Table 6 summarizes the assumed constants for the equation, the model and data vectors, and the solution. Figure 12 illustrates the solution with respect to the variable fraction of melt.

The solution implies that the andesite was emplaced when approximately 80 percent of the magma chamber was still molten, the granodiorite represented melts drawn off when the chamber was at 55 to 65 percent of its original volume, and the late-state bodies were extracted from the main chamber when approximately 27 percent remained. The

Table 6. Summary of inverse solution for isotopic data.

CONSTANTS		MODEL VECTOR INPUT	MODEL VECTOR OUTPUT	MODEL VECTOR 1 σ		DATA VECTOR B	DATA VECTOR $\hat{B}$	(i,j)
ϵ°_{m}(Nd) +7	Z (Nd)	-5	-6.17	0.56	ε (Sr,AND)	34.74	34.36	0.98
ϵ_{a} (Nd) -8.5	Z (Sr)	-5	-3.79	0.9	ε (Nd,AND)	-4.3	-4.3	0.99
ϵ°_{m}(Sr) 0	C°_{m} (Nd)	10	36.9	16.5	ε (Sr,GD1)	46.14	45.65	0.59
ϵ_{a} (Sr) 68.0	C°_{m} (Sr)	800	732	135	ε (Nd,GD1)	-6.5	-6.5	0.8
	f (AND)	8	0.79	0.04	ε (Sr,GD2)	45.42	47.6	0.6
	f (GD1)	0.6	0.65	0.04	ε (Nd,GD2)	-6.9	-6.8	0.79
	f (GD2)	0.5	0.64	0.03	ε (Sr,GDP)	57.33	55.66	0.72
	f (GDP)	0.4	0.55	0.07	ε (Nd,GDP)	-7.7	-7.9	0.53
	f (DIKE)	0.2	0.27	0.5	ε (Sr,DIKE)	67.12	67.13	0.98
					ε (Nd,DIKE)	-8.5	-8.5	0.98

a. The B vector represents the observed data. The $\hat{B}$ vector is the solution. (i,j) is the diagonal of the data information matrix. In this matrix a value of 1 implies a perfect fit of the model to the observations.

Figure 12. Epsilon Nd and Sr versus fraction of melt. Sample designation are as in Figure 3 (see pp. 25-27). The curves are generated from the model parameters found in Table 5 (see p. 43). The "goodness of fit" of the model to the data is apparent from the coincidence of the points to the lines. The solution implies that the andesite represents 80 percent melt remaining; the granodiorite, 65-55 percent melt remaining; and the late-stage dikes, 30 percent.

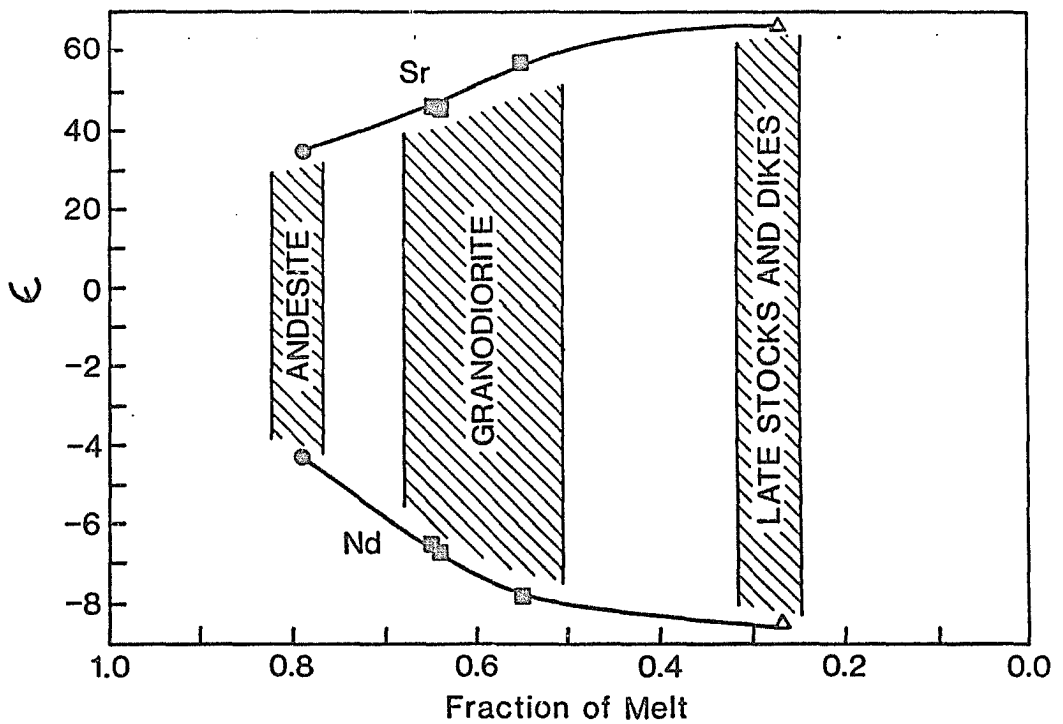

Figure 12. Epsilon Nd and Sr versus fraction of melt.

numeric modelling gives us our first insight into the size of the magma system which fed the igneous suite of Sierrita.

Solution of Z(Nd) and Z(Sr) allows estimation of the value for r according to the equation:

$$r = \frac{1 - D - Z}{1 - Z}$$

where

$$D = X_{min} K_d^{min}.$$

Taking the values of K_d from Table 2 (see p. 19) and modal analyses from Table 1 (see pp. 10-12) for two representative rocks (RS-MR-5 and RS-MR3-8), the values computed for r range from 0.6 to 0.9. These values are reasonable for melting in lower crustal environments where the ambient temperature may be within a few hundred degrees of the solidus (DePaolo, 1981a, Hon and Weill, 1982), or in areas, such as Sierrita, where a long history of igneous activity may have locally heated rocks above typical geotherms.

Numeric Solution of Trace Element Compositions

Figure 13 illustrates the rate of change of trace element compositions with respect to fraction of melt according to Equation 3 and assuming r to be 0.7. The most rapid changes in concentration happen within the first and last 15 percent of assimilation/crystallization. The intermediate

Figure 13. Concentration in the melt relative to original concentration versus fraction of melt for r = Ø.7. The diagram represents solution of Equation 3 in the text for different values of D, the bulk distribution coefficient, and CR, where CR is the ratio of the concentration in the assimilant to concentration in the original magma, i.e., Ca/Cm. The solid lines are for CR = Ø.1, the dashed lines for CR = 1Ø. The values of D are indicated for each curve. Note that the most rapid changes in concentrations of elements are in the first and last 1Ø to 15 percent of the process. The intermediate stages are characterized by slow changes for most elements.

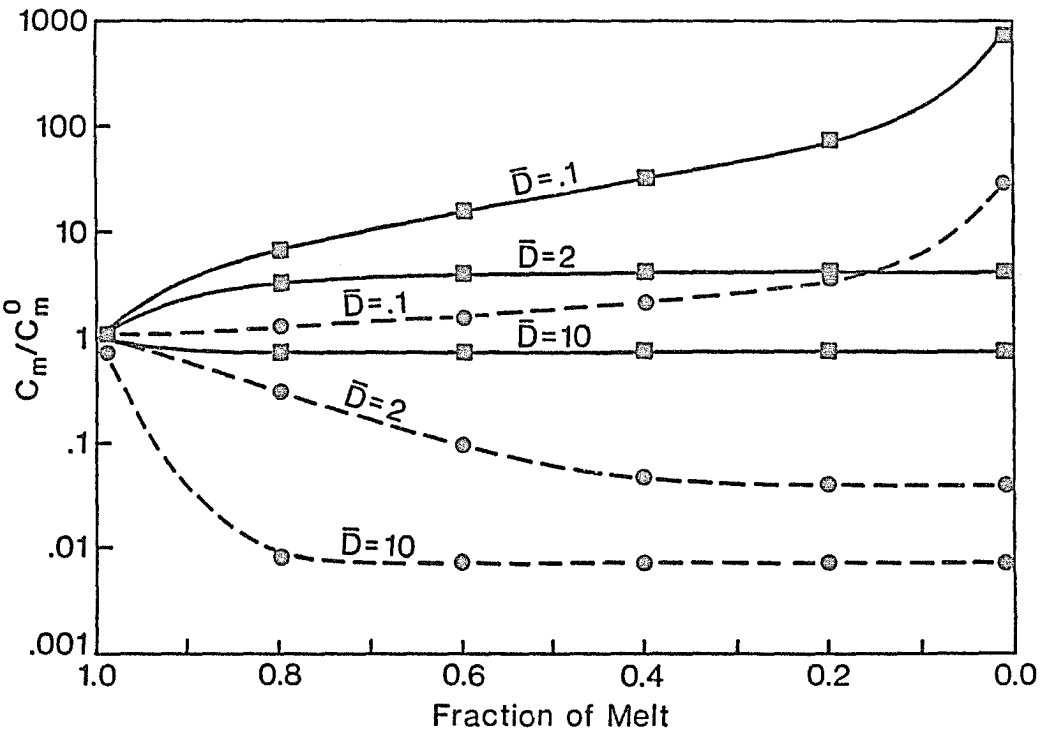

Figure 13. Theoretical elemental concentrations in melt versus fraction of melt for r=0.7.

stages of evolution are characterized by small changes in concentrations, an observation which agrees with the apparent similarity between samples analyzed (see Table 4, pp. 21-23 and Figure 7, p. 32).

Table 7 is a summary of the model and data vectors and the solution of Equation 3 using observed concentrations in samples from Sierrita and a value of r equal to Ø.7; Figure 14 shows concentrations of the elements relative to fraction of melt. The data vector was 2Ø entries long, and consisted of a solution for 4 elements in 5 rocks. The five "rocks" were an average of the andesite values (AND), two samples of the equigranular phase of the granodiorite (GD1 and GD2), the porphyritic phase of the granodiorite (GDP), and a late-stage plug (TWB). These are taken to be representative of the total system. Note that the value for fraction of melt for the andesite is Ø.63 compared to the Ø.79 obtained for the isotopic solution (see Table 6, p. 57) and that the late-stage porphyry bodies are Ø.34 versus the Ø.27 originally obtained. The granodiorite changes from a fraction of melt equal to Ø.55 to one of Ø.42-Ø.32. These changes in the granodiorite can be anticipated by the similarity in trace elements for the granodiorite (GD1, GD2, GDP) and porphyry plug (TWB) samples (see also Figures 7-8, pp. 32-33).

Table 7. Summary of inverse solution for the trace element data.

MODEL VECTOR					DATA VECTOR (a)			
	INPUT	OUTPUT		1 σ		B	$\hat{B}$	(I,J)
f (AND)	0.7	0.63		0.2	C (Co,AND)	13.7	13.9	1.6
f (GD1)	0.5	0.42		0.3	C (Th,AND)	6.6	6.9	1.1
f (GD2)	0.45	0.37		0.3	C (Rb,AND)	106	108	2.1
f (GDP)	0.42	0.32		0.3	C (Sm,AND)	4.8	4.8	3.1
f (TWB)	0.43	0.34		0.3	C (Co,GD1)	8.5	8.1	0.8
Z (Co)	-1	0.5	D = 0.2	1.2	C (Th,GD1)	10	9.8	0.4
Z (Th)	0.1	-0.2	0.5	0.7	C (Rb,GD1)	147	141	0.6
Z (Rb)	0.1	-0.3	0.5	1	C (Sm,GD1)	3.6	3.9	0.3
Z (Sm)	-1	-5.5	2.6	2.3	C (Co,GD2)	6.3	6.1	0.8
CR (Co)	0.1	-0.7	Ca = 20	0.9	C (Th,GD2)	11.9	10.6	0.4
CR (Th)	1.9	1.9	6.1	0.9	C (Rb,GD2)	142	149	0.4
CR (Rb)	13	12.6	775	0.8	C (Sm,GD2)	4	3.8	0.4
CR (Sm)	0.5	0.8	13.	1.3	C (Co,GDP)	3.8	3.5	0.9
C_m^o (Co)	19	19.4		2.2	C (Th,GDP)	12.1	11.5	0.6
C_m^o (Th)	2.7	3.2		1.1	C (Rb,GDP)	163	160	0.8
C_m^o (Rb)	5.5	63.6		1.6	C (Sm,GDP)	3.8	3.8	0.6
C_m^o (Sm)	26	17.2		14.8	C (Co,TWB)	3.7	4.5	0.9
					C (Th,TWB)	9.3	11.2	0.5
					C (Rb,TWB)	155	156	0.5
					C (Sm,TWB)	3.8	3.8	0.5

a. The B vector represents the observed data. The $\hat{B}$ vector is the solution. (I,J) is the diagonal of the data information vector.

Figure 14. Concentration in the melt/original concentration for the Sierrita igneous system. The curves represent solution of Equation 3 from the text, the points represent measured concentrations of the elements. The filled symbols at f=.6 are andesite, the filled symbols at 4=.4-.3 are granodiorite, the open symbols at 4=.3 are from one of the late-stage bodies. Table 7 (see p. 62) summarizes the information displayed in this figure. The "goodness of fit" of the model to the data is apparent from the coincidence of the points and the lines.

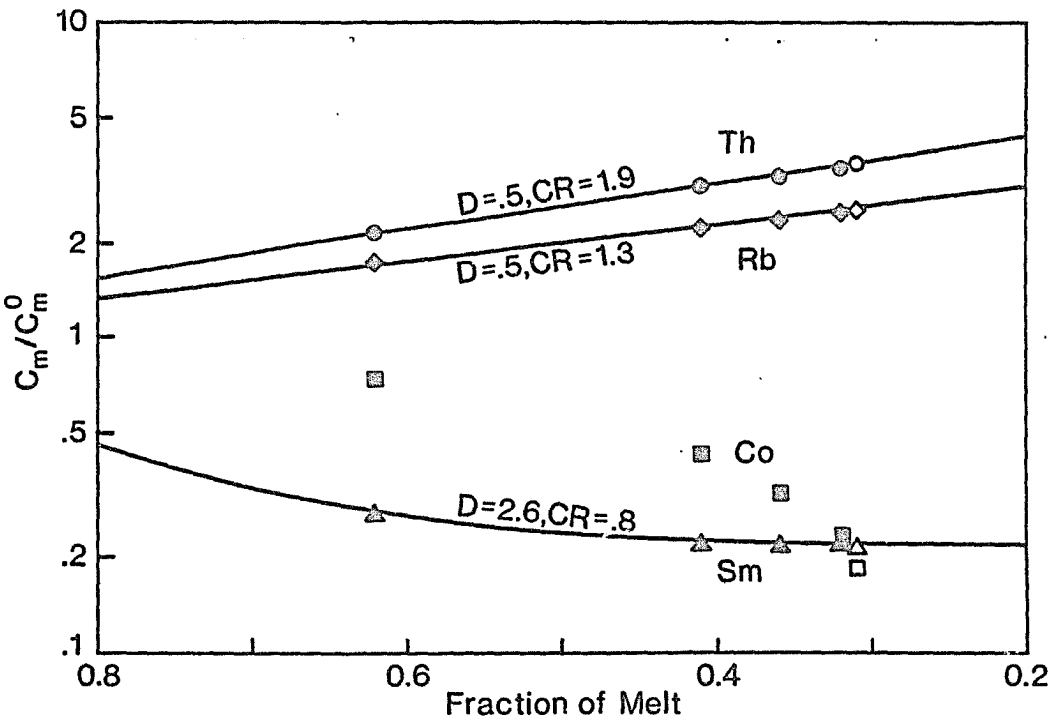

Figure 14. Elemental concentrations in melt versus fraction of melt for the inverse solution.

The solution gives reasonable values for initial concentration of the elements in a mantle-like melt, for the concentration of the elements in an amphibolitic assimilant, and for distribution coefficients (see Table 7, p. 62). There are however sizable uncertainties in some of the parameters of the model vector. These correspond to low values in the data information vector.

The matrix has not yet been inverted for all elements in all rocks because of numerical instabilities associated with the very slow rate of change of the concentrations for most elements; however, knowledge of CR, the ratio of the concentration in the assimilated material relative to the original magma, and Z, the weighted distribution coefficient, for the four elements allows one to estimate the values for fraction of melt for the other samples using Equation 3. These estimates are plotted against concentration in the liquid in Figure 15. Estimate of f will no doubt improve by inclusion of all data in the inverse matrix. Even this preliminary estimate allows one to see that, for certain elements such as the Ce and La, the late-stage bodies are non-continuous. Because rapid changes such as those observed for Ce and La are not permissible using the function represented in Equation 3, the assumption of constant Z, r, and CR are of questionable validity. In fact, perhaps one of the most persuasive arguments for

Figure 15. Concentration in the melt versus fraction of melt for various elements in the rocks from the Sierrita deposit. The values for f for the different samples were calculated using knowledge of CR and Z from Table 7 (see p. 62). For each element the first group of points represents the andesite samples, the second group of filled symbols the granodiorite, and the open symbols the late-stage dikes and porphyry bodies. Lines connecting the points are visual aids only because the actual curve which would represent the solution is non-linear, see for example Figure 12, p. 58, Figure 13, p. 60, and Figure 14, p. 63.

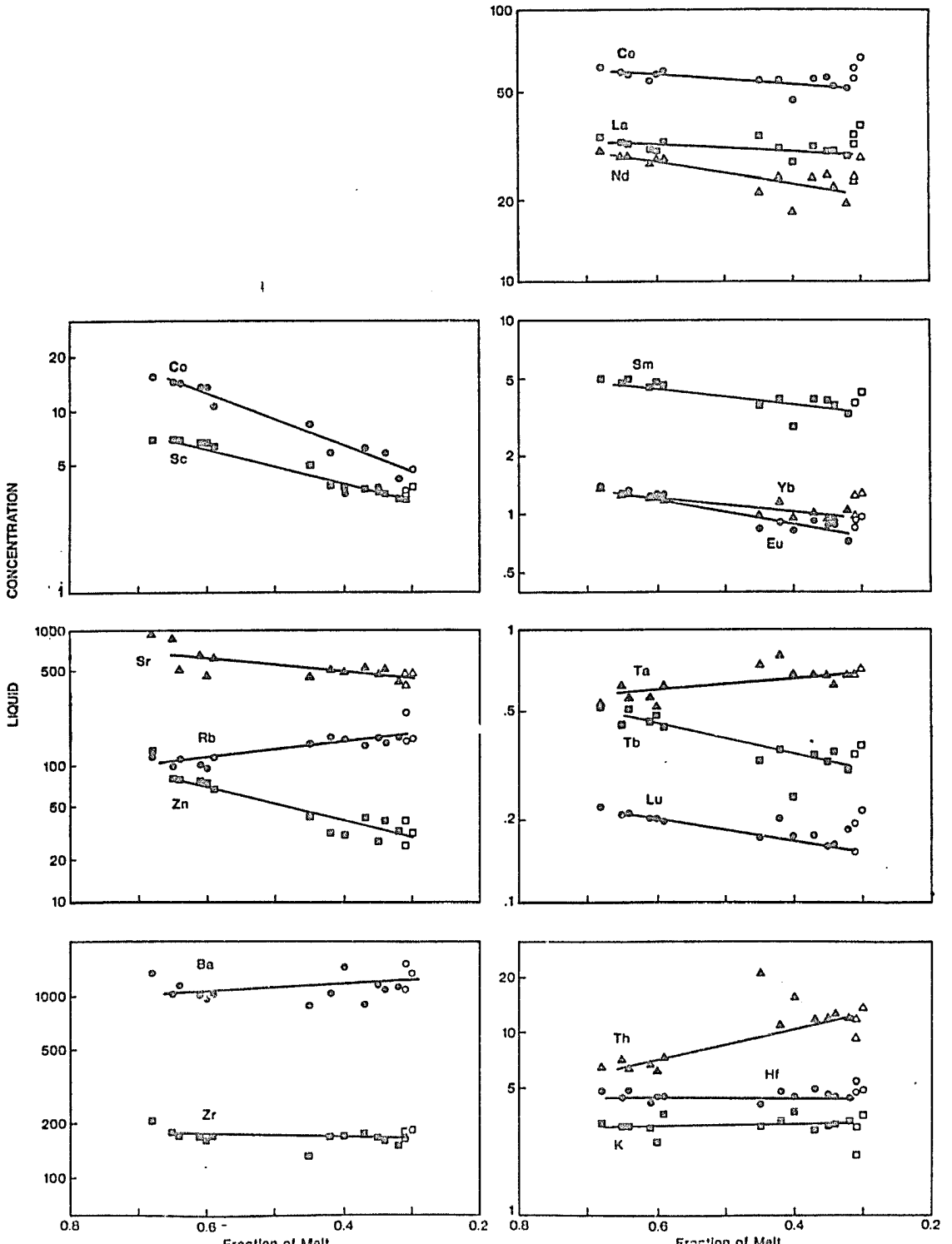

Figure 15. Estimates of fraction of melt represented by samples from Sierrita.

using inverse methods is that it allows characterization of solution space and detection of impermissible assumptions.

The percent crustal character represented by the samples can be calculated from the following equation:

$$\frac{f - 1}{(1 - 1/r)} = x$$

where x is mass of material which has been assimilated relative to the mass of the original magma, i.e., M_a/M_m^o. Using values of f, fraction of melt, from Table 6 (see p. 57) and r = Ø.7, the andesite is found to be approximately 5Ø percent crustal; granodiorite, 82 percent crustal; and late-stage bodies, completely crustal.

CHAPTER 6

DISCUSSION

The utility of the inverse method as a means of data analysis is that it yields a numerical solution to the proposed process -- that of assimilation and differentiation. The numerical solution in turn permits a test of the plausibility of the process, by seeing whether parameters are geologically reasonable, and also to estimate the size of the magmatic system. The porphyry bodies which localize mineralization are neither isolated nor confined to a small magmatic event. They are instead part of a continuum of magmatism which existed for some eight million years before their emplacement. Mineralization occurs at high levels in the magma system, and at these levels only a small portion of the total batholith which must exist at depth is sampled. As has been often suggested, the porphyry bodies do represent magmatic liquids from late stages of magmatic evolution, when approximately seventy percent of the original magma had crystallized. Because these bodies are fractured and mineralization occurs within the fractures, the ore solution must have invaded them still later.

This study demonstrates that the granites, and to a lesser extent the granodiorites, are crustal melts. Their geochemistry is characterized by crustal amphibolite rather than mantle peridotite. In the Southwest Pacific deposits (Hine and Mason, 1978, Mason and McDonald, 1978, Whalen et al., 1982) and at Silverbell deposit (Sawyer and Zartman, 1985), the intrusions also appear to have been derived from crustal materials. If this is a general characteristic of intrusion related to porphyry-copper mineralization, several important implications emerge.

The correlation between subduction zones and porphyry mineralization may exist because invasion of the continental crust by mantle-generated melts imparts enough heat to raise the ambient temperature above the solidus (Burnham, 1979). If melting occurred in water-undersaturated amphibolite, the solidus is in excess of 900°C (Wyllie, 1977). Perhaps it is the local generation of heat so much in excess of usual crustal temperatures, acting on rocks of amphibolite rather than granulite facies, that plays a role in generating the hydrous magmas appropriate to metallogenesis.

The possibility exists that the slope for the variation in oxygen fugacity reflects the hydrous nature of the magmas. Mueller (1971) has suggested that the oxygen fugacity in calc-alkaline magmas is buffered by water rather than the ferromagnesian minerals. Certainly the very gentle slope

of oxygen fugacity with respect to temperature for the Sierrita magmas suggests a buffer other than that of iron oxides. Magmas which may have had equally high oxygen fugacities but are inferred to have had lower water fugacities, such as those of the Sierra Nevada, generally are characterized by much steeper slopes of oxygen fugacity versus temperature (Speer, 1984).

The inference of crustal melting also implies that the distribution of mineralized systems may be a function of specific types of basement. In southeastern Arizona, the majority of deposits occur within the province characterized by 1.8 Ga basement (see Figure 11, p. 50 and Titley, 1982a). A question which must be addressed within this context is to what extent the lithology of basement is particularly suited to generation of the appropriate melts, and to what extent other conditions, such as structural setting, control the appropriate development of the system.

Titley and Beane (1981) and Meyer (1981) emphasize that porphyry copper deposits are not found in thickened continental crust but rather at cratonic edges, and in "mobile zones" (Titley and Beane, 1981) between Precambrian craton and the "outboard" batholiths, such as the Peninsular Ranges.

Candela and Holland (1986) have discussed the fact that the timing of vapor exsolution is controlled by the

depth of magma emplacement and initial water content. They reason that if copper is a compatible element and molybdenum incompatible, early vapor exsolution, resulting from either high initial water content or high-level emplacement such as would be possible in an extensional environment, will favor development of a copper-rich fluid rather than one enriched in molybdenum. Newberry and Swanson (1985) concur that the structural setting is of primary importance in generation of tungsten, as contrasted to copper deposits. They argue that deep intrusion and a high pressure environment would lead to late vapor exsolution and consequent enrichment of the fluid in the incompatible element tungsten relative to the base metals.

Perhaps conditions in southern Arizona combined to be favorable: there existed an amphibolitic basement and the structures which localize the intrusions are interpreted to have been extensional. The local extensional structures were created in the offsets of major faults, because the faults were oriented obliquely with respect to the major compressional axes (Titley et al, 1978, Heidrick and Titley, 1982).

However, in order to assess the relative importance of these factors, we must have more studies which characterize the specific kind of crust for various deposits. Can the intrusions related to copper deposits be generated from

felsic sources such as gneisses, and what is the character of source regions associated with molybdenum mineralization?

Finally, this study has addressed the nature of magmatism at convergent plate boundaries. Other work has demonstrated that batholithic granitoid bodies become increasingly crustal in character inboard of a trench (Farmer and DePaolo, 1984), and also that igneous complexes are sometimes the result of mixing of mantle and crustal melts (Halliday et al., 1980, McCulloch and Chappell, 1982, Patchett and Bridgwater, 1984, Frost and O'Nions, 1985). The present work contributes to the growing body of data which suggests that within a single sequence of rocks progressive differentiation is coupled to assimilation (Taylor, 1980, DePaolo, 1981a, 1981b, Ben Othman et al., 1984). Isotopic studies have, of course, been crucial in uncovering this evidence because the trends in chemical components mimic those which would result from differentiation alone. It will remain for further combined trace element and isotopic studies to evaluate how common this process has been.

APPENDIX I

ANALYTICAL METHODS

All samples were crushed in aluminum foil boats, hand-picked so as to avoid weathered and altered surfaces, and powdered in a chrome steel shatterbox. To test for representativeness of sample size, large pieces of granodiorite (ca. 30 cm on a side) were broken into fist-sized fragments and divided into four piles. Two of the four piles were processed independently. The disagreement between split 1 and split 2 is calculated according to:

$$\text{delta \%} = \frac{\text{split 1} - (\text{split 1} + \text{split 2})/2 \times 100}{(\text{split 1} + \text{split 2})/2} \qquad (4)$$

The splitting procedure was done on three different large samples, two of which were the porphyritic phase of the granodiorite. The average disagreement, or average delta percent, for the three samples is shown in Column 2 of Table 8. The small deviations imply that although trace elements in granites reside primarily in accessory minerals (Gromet and Silver, 1983, Mittlefehldt and Miller 1983, Fourcade and Allegre, 1981), the sample size was large enough to include representative amounts of accessory phases.

Table 8. Estimates of precision and accuracy.

	Chrome Steel a	Sample Splits b	Powder Splits c	"Accuracy" W1	G1 d	NBS 278
Na	3.541	1.9	1.2	3.2	1.8	-0.1
K	15.164	6.1	1.2	6.6	-7.0	-4.6
Ca	87.440	3.0	1.0	0.8	-7.1	3.6
Sc	0.097	1.4	0.8	1.6	-0.2	-3.8
Mn	6.300	0.9	n.d.	2.8	-7.8	-3.7
Fe	831.340	2.3	0.8	-0.1	-5.1	0.7
Co	0.226	1.1	1.0	0.6	-15.0	-0.7
Zn	0.630	0.9	1.6	-1.1	5.3	-10.9
Rb	0.036	1.8	0.8	0.7	-1.3	0.2
Sr	0.135	1.5	1.2	0.4	-1.2	-13.0
Zr	0.725	2.4	3.7	-1.8	8.7	3.3
Cs	0.024	1.1	0.7	9.7	-3.9	n.r.
Ba	2.016	9.1	0.5	3.9	0.6	-17.4
La	0.132	7.0	0.8	0.7	-1.4	-9.6
Ce	0.232	6.2	0.7	-4.5	2.9	1.4
Nd	0.070	5.4	0.5	-12.0	2.3	-0.1
Sm	0.022	5.0	1.8	-8.2	-5.4	-1.4
Eu	0.003	1.8	0.5	-3.2	-4.4	3.5
Tb	0.004	3.2	4.0	-9.3	-17.7	-21.5
Yb	0.012	1.2	0.8	-3.1	2.1	-1.9
Lu	0.002	1.6	0.5	1.5	0.0	-10.6
Hf	0.005	1.4	0.8	-0.8	7.5	-8.4
Ta	0.001	2.5	2.0	-17.0	5.4	-0.4
Th	0.010	2.3	1.2	-9.2	2.0	-0.2
U	0.006	7.2	0.6	-2.6	16.6	-1.1

a. Contamination (in ppm) from sample preparation in chrome steel shatterbox
b. Average percent difference between splits of porphyritic samples.
c. Average percent difference between splits of powders.
d. Average percent difference between reported and observed values for the standard rocks.

Brazilian optical quartz was run through the shatterbox in order to assess contamination. The most serious contamination was of course the chromium and, based on expected values for chromium in these rocks (20-50 ppm) compared to obtained values (100-150 ppm), contamination is estimated to be an average of 100 ppm. The absolute amount of contamination seems to depend on the amount of quartz in the sample, this is explained by the fact that quartz is the only major mineral constituent with a hardness greater than the chrome steel of the shatterbox. Because a correction for chromium would have to be weighted with respect to modal quartz, the values for chromium in samples are not reported. The values for contamination of other elements, based on the Brazililan quartz and normalized to 100 ppm chromium, are listed in Column 1 of Table 8 (see p. 73). It is apparent from the table that contamination is not an appreciable part of the total concentration.

Trace Element Analysis

Samples were irradiated for three hours at a flux of 7×10^{11} neutrons/cm^2/sec in the TRIGA reactor at the University of Arizona. Chemical standards and five standard rocks (BCR-1, NBS 688, W-1, G-1, and NBS 278) were included in the irradiation. Counting and data reduction were done at the Gamma-ray Laboratory at the University of Arizona, which is under the direction of W. V. Boynton. Samples

were counted, using an anti-Comptom spectrometer, for 8 hours in the period 5 to 10 days after irradiation and again for 4 hours 30-40 days after irradiation. The average uncertainties listed in the final column of Table 4 (see pp. 21-23) are as percent relative error and represent estimates of one standard deviation from the mean. They are calculated from multiple determinations, often of more than one peak, for each element.

Instrumental reproducibility is reported in column 3 of Table 8 (see p. 73). It represents the percent disagreement using Equation 4 between aliquots of the same powder run during the same irradiation and successive irradiations. Three different powders, that is six aliquots, have been analyzed and the values in Table 8 are the average disagreement for the three different samples.

An estimate of accuracy is included in columns 4 through 6 of Table 8. These values represent the percent deviation from the reported values (Gladney et al, 1983, Graham et al, 1982, NBS Certification and NBS information), according to the equation:

$$\text{delta } \% = (\text{observed}-\text{reported})/\text{reported} \times 100. \qquad (5)$$

The values in Table 8 are the average of two such calculations for each standard rock.

Major Element Analysis

Major element determinations were performed on the same powders as those used for the neutron activation analysis. Analyses were done by Inductively Coupled Plasma method at Skyline Laboratories in Tucson, Arizona and X-ray fluorescence by XRAL of Canada.

Isotope Analyses

Sm/Nd and Rb/Sr isotopic compositions were analyzed in the Department of Geosciences, University of Arizona, under the direction of P.J. Patchett. Nine samples were selected which represented the range of chemical diversity in the igneous suite. These included two samples of the Demetrie Andesite, one each of the quartz diorite, the Red Boy Rhyolite, the equigranular phase of the Ruby Star Granodiorite, the porphyritic phase of the granodiorite, the granite porphyry, and quartz latite dike. Only those known from their major and trace element chemistry to be reasonably free from the effects of hydrothermal alteration were included. Two samples from the same hand-specimen of the equigranular Ruby Star were analyzed in order to have some feeling for the representativeness of the sample size. These duplicate powders are listed in Table 3 (see p. 20) as RS-MR-5 and RS-MR-5x. All samples were run for Sm and Nd, six of the nine for Rb and Sr.

After a series of initial dissolutions of the powders, all samples were heated in hydrothermal bombs for one week to assure complete dissolution of accessory minerals. Rubidium, strontium, and an aliquot of the rare earth elements were separated on AG50W-X12 resin. Samarium and neodymium were then separated using Teflon powder coated with di-2-ethylhexyl orthophosphoric acid.

Sr and Rb were loaded onto single Ta filaments using H_3PO_4. Sm and Nd were loaded on both side filaments of a three Re filament assembly. The mass spectrometer used was a fully automated VG Model 354 with multi-collector capability. The spectrometer was programmed to collect data on naturally occurring isotopes in addition to the masses of interest in order to monitor the quality of data. The statistics reported in Table 3 (see p. 20) represent estimates of 2 standard deviations from the mean; they were determined from multiple blocks of data collected on each sample. Further discussion of the analytical procedure may be found in White and Patchett (1984).

For the period of analysis, determinations of the La Jolla standard yielded $^{143}Nd/^{144}Nd = .511866 \pm 14$ and of the Sr standard NBS-987 gave $^{87}Sr/^{86}Sr = .710241 \pm 46$. Both of these errors again represent 2 standard deviations from the mean. Three aliquots of the potassium feldspar standard were analyzed, and they yielded a value of Sr of $65.52 \pm .27$

and Rb of 528.Ø1±15.73 (1 standard deviation), versus reported values of 65.485±.32 and 523.9±1 respectively. The large standard deviation for the Rb determinations were due to the procedure of mounting the Rb on a single center filament. This causes poor ion emission stability and rapid ionization of all material on the filament. However, based on results obtained for KS-6Ø7 and also comparison of INAA and isotope dilution analyses of samples, the values reported for Rb appear to be within approximately 3 percent of expected values, and thus the uncertainty in the correction to initial Sr ratios is very small.

REFERENCES

Anders, E., Ebihara, M. (1982) Solar system abundances of the elements. Geoch. Cosmoch. Acta 46, 2363-2380.

Anthony, E. Y., Titley, S. R. (in prep.) Characteristics of highly differentiated rocks in an oxiding, I-type igneous suite.

Arth, J. G. (1976) Behavior of trace elements during magmatic processes -- A summary of theoretical models and their applications. Jour. Res. U.S. Geol. Survey 4, 41-47.

Banks, N.G., Cornwall, H.R., Silberman, M.L., Creasey, S.C., Marvin, R. F. (1972) Chronology of intrusion and ore deposition at Ray, Arizona: Part I, K-Ar ages. Econ. Geol. 67, 864-878.

Ben Othman, D., Fourcade, S., Allegre, C.J. (1984) Recycling processes in granite-granodiorite complex genesis: the Querigut case studied by Nd-Sr isotope systematics. Earth Planet. Sci. Letters 69, 290-300.

Burnham, C.W. (1979) Magmas and hydrothermal fluids. In Geochemistry of hydrothermal ore deposits (ed. H.L. Barnes), pp. 71-136. John Wiley and Sons.

Burnham, C.W., Ohmoto, H. (1980) Late stage processes of felsic magmatism. In Granitic magmatism and related mineralization (eds. S. Ishihara and S. Takenouchi), pp. 1-11. Mining Geol. Japan.

Burnham, C.W., Holloway, J.R., Davis, N.F. (1972) Thermodynamic properties of water to 1000 C and 10,000 bars. Geol. Soc. Am. Spec. Paper 132.

Candela, P.A., Holland, H.D. (1986) A mass transfer model for copper and molybdenum in magmatic hydrothermal systems: the origin of porphyry-type ore deposits. Econ. Geol. 81, 1-19.

Chivas, A.R. (1981) Geochemical evidence for magmatic fluids in porphyry copper mineralization. Part I. Mafic silicates from the Koloula igneous complex. Contrib. Mineral. Petrol. 78, 389-403.

Cooper, J.R. (1960) Some geological features of the Pima mining district. U.S.G.S. Bull. 1112-C, 63-103.

Cooper, J.R. (1971) Mesozoic stratigraphy of the Sierrita Mountains, Pima County, Arizona. U.S.G.S. Prof. Paper 658-D, 1-42.

Cooper, J.R. (1973) Geologic map of the Twin Buttes Quadrangle southwest of Tucson, Pima County, Arizona. U.S.G.S. Map I-745.

DePaolo, D.J. (1981a) Trace element and isotopic effects of combined wallrock assimilation and fractional crystallization. Earth Planet. Sci. Letters 53, 189-202.

DePaolo, D.J. (1981b) A neodymium and strontium isotopic study of mesozoic calc-alkaline granitic batholiths of the Sierra Nevada and Peninsular Ranges, California. Journ. Geophys. Res. 86, 10470-10488.

Drake, M.J. (1975) The oxidation state of europium as an indicator of oxygen fugacity. Geoch. Cosmoch. Acta 39, 55-64.

Drake, M.J., Weill, D.F. (1975) Partition of Sr, Ba, Ca, Y, Eu^{2+}, Eu^{3+}, and other REE between plagioclase feldspar and magmatic liquid: an experimental study. Geoch. Cosmoch. Acta 39, 689-712.

Dyar, M.D. (1985) personal written communication June 12, Massachusetts Institute of Technology, Cambridge, Massachusetts.

Farmer, G.L., DePaolo, D.J. (1984) Origin of Mesozoic and Tertiary granite in the western United States and implications for pre-Mesozoic crustal structure 2. Nd and Sr isotopic studies of unmineralized and Cu- and Mo-mineralized granite in the Precambrian craton. Jour. Geophys. Res. 89, 10141-10160.

Fourcade, S., Allegre, C.J. (1981) Trace elements behavior in granite genesis: A case study - The calc-alkaline plutonic association from the Querigut complex (Pyrenees, France). Contrib. Mineral. Petrol. 76, 177-195.

Frost, C.D., O'Nions, R.K. (1985) Caledonian magma genesis and crustal recycling. Jour. Petrol. 26, 515-544.

Gilmour, P. (1982) Grades and tonnages of porphyry copper deposits. In Advances in geology of the porphyry copper deposits (ed. S.R. Titley), pp. 7-35. Univ. of Ariz. Press.

Gladney, E.S., Burns, C.E., Roelandts, I. (1983) 1982 compilation of elemental concentrations in eleven United States Geological Survey rock standards. Geostandards Newsletter 7, 3-226.

Goldstein, S.L., O'Nions, R.K., Hamilton, P.J. (1984) A Sm-Nd isotopic study of atmospheric dusts and particulates from major river systems. Earth Planet. Sci. Letters 70, 221-236.

Graham, C.C., Glascock, M.D., Carni, J.J., Vogt, J.R., Spaulding, T.G. (1982) Determination of elements in National Bureau of Standards' geological Standard Reference Materials by neutron activation analysis. Anal. Chem. 54, 1623-1627.

Gromet, L.P., Silver, L.T. (1983) Rare earth element distributions among minerals in a granodiorite and their petrogenetic implications. Geoch. Cosmoch. Acta 47, 925-939.

Grove, T.L., Baker, M.B., Donnelly-Nolan, J.M. (1985) Quantitative estimates of assimilation and fractional crystallization (AFC) in calc-alkaline systems. Geol. Soc. Am. abstr. 17, 599.

Halliday, A.N., Stephens, W.E., Harmon, R. S. (1980) Rb-Sr and O isotopic relationships in 3 zoned Caledonian granitic plutons, Southern Uplands, Scotland: evidence for varied sources and hybridization of magmas. J. Geol. Soc. London 137, 329-348.

Hanson, G.N. (1978) The application of trace elements to the petrogenesis of igneous rocks of granitic composition. Earth Planet. Sci. Letters 38, 26-43.

Hawkesworth, C.J., Norry, M.J., Roddick, J.C., Baker, P.E. (1979) $^{143}Nd/^{144}Nd$, $^{87}Sr/^{87}Sr$., and incompatible element variations in calc-alkaline andesites and plateau lavas from South America. Earth Planet. Sci. Letters 42, 45-57.

Heidrick, T.L., Titley, S.R. (1982) Fracture and dike patterns in Laramide plutons and their structural and tectonic implications. In Advances in Geology of the porphyry copper deposits (ed. S.R. Titley), pp. 73-92. Univ. of Ariz. Press.

Hess, N.J. (in prep.) Phase equilibria studies of the Ruby Star Granodiorite, Sierrita district, Arizona. M.S. thesis, Univ. of Arizona.

Hess, N.J., Anthony, E.Y., Titley, S.R., (in prep.) Oxidation state of porphyry copper magmas as deduced from biotite, potassium feldspar, and magnetite equilibria.

Hine, R., Mason, D.R. (1978) Intrusive rocks associated with porphyry copper mineralization, New Britain, Papua New Guinea. Econ. Geol. 73, 749-760.

Hon, R., Weill, D.F. (1982) Heat balance of basaltic intrusion vs. granitic fusion in the lower crust. EOS 63, 470.

Koski, R.A., Cook, D.S. (1982) Geology of the Christmas porphyry copper deposit: Gila County, Arizona. In Advances in geology of the copper deposits (ed. S.R. Titley), pp. 353-374. Univ. of Ariz. Press.

Marvin, R.F., Stern, T.W., Creasey, S.C., Mehnert, H.H. (1973) Radiometric ages of igneous rocks from Pima, Santa Cruz, and Cochise Counties, southeastern Arizona. U.S. Geol. Survey Bull. 1379, 27 p.

Mason, D.R. (1978) Compositional variations in ferromagnesian minerals from porphyry copper-generating and barren intrusions of the Western Highlands, Papua New Guinea. Econ. Geol. 73, 878-890.

Mason, D.R., McDonald, J.A. (1978) Intrusive rocks and porphyry copper occurrences of the Papua New Guinea-Solomon Islands region: a reconnaissance study. Econ. Geol. 73, 857-877.

McBirney, A.R. (1983) personal communication, Professor, University of Oregon, Eugene, Oregon.

Meyer, C. (1982) Ore-forming processes in geologic history. Econ. Geol. (75th anniv. vol.), 6-41.

Minster, J.F., Minster, J.B., Treuil, M., Allegre, C.J. (1977) Systematic use of trace elements in igneous processes - II. Inverse problem of the fractional crystallization process in volcanic suites. Contrib. Mineral. Petrol. 61, 49-77.

Mittlefehldt, D.W., Miller, C.F. (1983) Geochemistry of Sweetwater Wash pluton, California: Implications for "anomalous" trace element behavior during differentiation of felsic magmas. Geoch. Cosmoch. Acta 47, 109-124.

McCulloch, M.T., Chappell, B.W. (1982) Nd isotopic characteristics of S- and I-type granites. Earth Planet. Sci. Letters 58, 51-64.

Mueller, R.F. (1971) Oxidative capacity of magmatic components. Amer. Jour. Sci. 270, 236-243.

Naney, M.T. (1983) Phase equilibria of rock-forming ferromagnesian silicates in granitic systems. Amer. Jour. Sci. 283, 993-1033.

Newberry, R.J., Swanson, S.E. (1985) Granites associated with tungsten skarns. In Granite-related mineral deposits (ed. Taylor, R.P., Strong, D.F.) pp. 197-199. CIM Conference.

Nicholls, I.A., Harris, K.L. (1980) Experimental rare earth element partition coefficients for garnet, clinopyroxene, and amphibole coexisting with andesitic and basaltic liquids. Geochem. Cosmoch. Acta 44, 287-308.

Noyes, H.J., Frey, F.A., Wones, D.R. (1983a) A tale of two plutons: geochemical evidence bearing on the origin and differentiation of the Red Lake and Eagle Pass plutons, central Sierra Nevada, California. Jour. Geol. 91, 487-509.

Noyes, H.J., Wones, D.R., Frey, F.A. (1983b), A tale of two plutons: petrographic and mineralogical constraints on the petrogenesis of the Red Lake and Eagle Pass plutons, central Sierra Nevada, California. Jour. Geol. 91, 353-379.

O'Hara, M.J. (1984) Continuous partial melting regimes in the upper mantle, refilled-tapped-fractionated (RTF) magma chambers, and the evolution of chondrite or whole-earth normalised trace element concentration patterns (spidergrams) for igneous magmas and residua. Proc. Taos Conf. Open Magma Systems.

Patchett, P.J., Bridgwater, D. (1984) Origin of continental crust of 1.9-1.7 Ga age defined by Nd isotopes in the Ketilidian terrain of south Greenland. Contrib. Mineral. Petrol. 87, 311-318.

Sawyer, D.A., Zartman, R.E. (1985) Lead isotopes in continental arc magmas and origin of porphyry Cu deposits in Arizona. Geol. Soc. Am. abstr. 17, 708.

Shafiqullah, M., Langlois, J.D. (1978) The Pima mining district, Arizona - a geochronological update. New Mexico Geol. Soc. Guidebook, 29th Field Conf., 321-327.

Speer, J.A., (1984) Micas in igneous rocks. In Reviews in Mineral. 13 (ed. S.W. Bailey), 299-356.

Streckeisen, A.L. (1973) Plutonic rocks - classification and nomenclature. Geotimes 18, 26-30.

Taylor, H.P., Jr. (1980) The effects of assimilation of country rocks by magmas on 18O/16O and $^{87}Sr/^{86}Sr$ systematics in igneous rocks. Earth Planet. Sci. Letters 47, 243-254.

Titley, S.R., Thompson, R.C., Haynes, F.M., Manske, S.L., Robison, L.C., White, J.L. 1986, Evolution of fractures and alteration in the Sierrita-Esperanza hydrothermal system, Pima County, Arizona, Econ. Geol., 81, in press.

Titley, S.R. (1982a) Geologic setting of porphyry copper deposits. In Advances in geology of the porphyry copper deposits (ed. S.R. Titley), pp. 37-58. Univ. of Ariz. Press.

Titley, S.R. (1982b) Some features of tectonic history and ore genesis in the Pima mining district. In Advances in geology of the porphyry copper deposits (ed. S.R. Titley), 387-406. Univ. of Ariz. Press.

Titley, S.R., Beane, R.E. (1981) Porphyry copper deposits. Econ. Geol. (75th anniv. vol.), 214-269.

Titley, S.R., Fleming, A.W., Neale, T.I. (1978) Tectonic evolution of the porphyry copper system at Yandera, Papua New Guinea. Econ. Geol. 73, 810-828.

Watson, E.B. (1982) Basalt contamination by continental crust: some experiments and models. Contrib. Mineral. Petrol. 80, 73-87.

West, R.J., Aiken, D.M. (1982) Geology of the Sierrita-Esperanza deposit. In Advances in geology of the porphyry copper deposits (ed. S.R. Titley), 433-466. Univ. of Ariz. Press.

Whalen, J.B., Britten, R.M., McDougall, I. (1982) Geochronology and geochemistry of the Frieda River prospect area, Papua New Guinea. Econ. Geol. 77, 592-616.

White, W.W., Patchett, J. (1984) Hf-Nd-Sr isotopes and incompatible element abundances in island arcs: implications for magma origins and crust-mantle evolution. Earth Planet. Sci. Letters 67, 167-185.

Winkler. H.G.F. (1979) Petrogenesis of metamorphic rocks. Springer-Verlag. 348 p.

Wones, D.R. (1972) Stability of biotite: a reply. Amer. Mineral. 57, 316-317.

Wyllie, P.J. (1977) Crustal anatexis: an experimental review. Tectonophysics 43, 41-71.